FACULDADE DE ENGENHARIA DA UNIVERSIDADE DO PORTO

On the Mechanical and Electrochemical Performance of High Corrosion Resistance WC-Ni-based Composites

Tiago Pinto de Freitas de Sousa Guedes

Mestrado em Engenharia de Materiais - Especialização em Metalurgia
Supervisor: Dr. Rúben Santos

July 7, 2022

Resumo

O metal duro, mais concretamente o Carboneto de Tungsténio, é frequentemente utilizado em situações onde existe uma necessidade de uma elevada resistência ao desgaste. A utilização deste material aumenta consideravelmente a eficiência da produção pois cria vantagens competitivas que prolongam a vida útil do material e a sua eficácia. Tanto na terra como no mar, humidade, água, areia e sólidos abrasivos causam um enorme desgaste. Ao utilizar o metal duro minimiza-se esse desgaste. Na indústria do petróleo, gás e petroquímica, observa-se a aplicação de ligas de metal duro em meios alcalinos, tais como a água do mar. É por isso relevante obter conhecimento sobre ligas que possuem resistência elevada a estes meios. Ao incidir sobre uma melhoria na resistência à corrosão, estamos a comprometer na resistência ao desgaste, no entanto, esta permuta compensa, pois é a corrosão que fará com que a vida útil do material diminua.

O objetivo desta dissertação é analisar e validar as propriedades mecânicas e eletroquímicas de graus de ligas de metal duro previamente estudadas na bibliografia e que se demonstraram promissoras face a ambientes corrosivos, fazendo assim a substituição e a possível eliminação total ou parcial do cobalto nas ligas de metal duro.

Através da medição de dureza e cálculo da tenacidade à fratura, é possível tirar conclusões sobre a resistência ao desgaste de um determinado material. É realizada ainda a avaliação da resistência à corrosão através de uma série de ensaios eletroquímicos que permitiram tirar conclusões sobre a resistência à corrosão das ligas estudadas.

É realizada ainda uma seriação das amostras e um processo de análise comparativo de forma a catalogar eficientemente as ligas com características mais promissoras para aplicações em água do mar.

Abstract

Hard metals, or cemented carbides, specifically Tungsten Carbide (WC), are often used in situations where there is a need for high wear resistance. The use of this material considerably increases production efficiency as it creates competitive advantages that extend the material's useful life and effectiveness. Both on land and in the sea, moisture, water, sand, and abrasive solids cause enormous wear and tear on materials. By using cemented carbides, this wear is minimized. In the oil, gas and petrochemical industry, the application of carbide alloys in alkaline media, such as seawater, is observed. It is therefore relevant to obtain knowledge about alloys that have high resistance to these media. By focusing on an improvement in corrosion resistance, we are compromising on wear resistance, however, this trade-off pays off as it is corrosion that will cause the material's lifespan to decrease.

The objective of this dissertation is to analyse and validate the mechanical and electrochemical properties of grades of carbide alloys previously studied in the bibliography and which have shown to be promising in the face of corrosive environments, thus making the replacement and possible total or partial elimination of cobalt in alloys of hard metal.

By measuring hardness and calculating fracture toughness, it is possible to conclude the wear resistance of a given material. An evaluation of corrosion resistance is also carried out through a series of electrochemical tests that allowed conclusions to be drawn about the corrosion resistance of the alloys studied.

A seriation of samples and a comparative analysis is also carried out to efficiently chart the alloys with the most promising characteristics for applications in seawater.

Agradecimentos

Entregar esta dissertação representa o culminar de um ciclo de estudos. O fim de uma etapa. O início de novas experiências. Esta foi uma etapa muito importante, a qual eu agradeço muito por ter tido a oportunidade de concluir. Quero por isso, entregar algumas palavras de agradecimento a todos aqueles que me direcionaram neste caminho que agora chega ao fim e que tornaram tudo possível.

O meu maior e mais sincero obrigado vai para a minha mãe. Ela que sempre suportou os meus estudos e sempre fez questão que não me faltasse nada para tal. Um grande muito obrigado por toda a força que me deste, pela tua presença e disponibilidade, e por estares sempre pronta a me ajudar a crescer e ouvir as minhas teorias e opiniões sobre o mundo da engenharia que pouco ou nada te interessam.

Ao meu pai um sincero obrigado, por toda a força e por sempre querer saber quando é que eu acabo isto. Um exemplo a seguir, que leva tudo até ao fim. Alguém trabalhador e empenhado, que nunca desiste de nada e que sempre faz questão que tenhamos o melhor jantar das nossas vidas, todas as semanas.

À minha tia Isabel que sempre alimentou o meu vício pelos brinquedinhos, e sempre me ajudou em tudo o que pode. A sua grande preocupação sempre foi ver-me feliz e é sempre a primeira a ajudar quando eu preciso. Sempre acreditou em mim e sempre soube que vou ter muito sucesso. Talvez por sermos dois aquários.

Ao meu irmão Pedro, esse louco pelo mundo e pelo desporto automóvel, que sempre se mostrou disponível para me levar para Penafiel para montar e desmontar o Saxo de rally, que coitadinho, anda sempre em trabalhos. Apesar de uma vida atarefada, sempre arranja tempo para irmos jantar ao velhinho e me vir buscar às 8 da manhã para ir ver o Rally de Portugal ou os regionais. Ele que sempre alimentou minha fome pela Engenharia, mesmo que nem sempre o saiba.

A todos os meus amigos que sempre acreditaram em mim e nunca duvidaram das minhas capacidades como aspirante a Engenheiro.

À Maria Eduarda, que incansavelmente me motiva todos os dias, “vamos, está quase”, “vai tudo correr bem”, “tu consegues”. A todo o carinho que sempre me mostrou e toda a confiança depositada que me permitiu ser o melhor de mim mesmo. Um grande muito obrigado.

Por fim, um grande agradecimento ao professor Dr. Rúben Santos, orientador desta dissertação. Ele que sempre se mostrou disponível para esclarecer todas e qualquer dúvida que eu tivesse e sempre arranjou tempo para mim. Foi um prazer trabalhar consigo.

Tiago Sousa Guedes

“The search for knowledge will forever be infinite”

Tiago Sousa Guedes, 2022

Contents

Chapter 1

1. Introduction

Nowadays, there is a great need for tungsten carbide (WC)-based composites applications. A large number of industries, mainly oil, gas, and petrochemical are focusing on finding more ways of using these composites to extend the tools' work life.

Powder metallurgy has been growing a lot in recent years due to an increasing need for WC-based composites use in the industries thanks to their unique combination of properties [1].

Cemented carbides, in particular hard metals (HD), are one of the most promising subfamilies of cermets. Their microstructure is specifically constituted by grains of a transition metal carbide, embedded in a metallic matrix that acts as a binder.

WC-Co is extremely relevant due to the combination of high hardness and wear resistance, a typical property of ceramics (WC), and a high toughness of metals (Co), thus creating a coalition that becomes the standard in many industries [2,3].

The main binder used in carbide alloys is Co [4], due to its excellent mechanical properties and ease of processing. Co, has very high wettability towards WC, thus providing a very strong adhesion. It also gives the alloy high hardness, and toughness. However, the use of Co brings serious problems regarding the performance of the alloys in corrosive media, especially when dealing with acidic environments. Other disadvantages that motivate R&D in finding substitute binders for Co are its high toxicity, rising price, and geopolitical issues involved in its extraction [5]. Another drawback regarding the use of Co as a binder in WC-based composites is its poor performance in acidic media, typical for oil, gas, and petrochemical applications, where the composite is subjected to both corrosion and wear. In these environments, the corrosive media accelerates the failure of the machinery and tools, which leads to more recurring maintenance, and elevates the overall running costs [6].

In alternative to Co, other binders are utilized, when there is a need for better corrosion resistance. A range of WC grades with Ni and Cr binders are already being used in the industry and they confer a much better response when there is a need for higher corrosion performance in acidic media [7]. In stainless steels, the effects of Ni-Cr confer high corrosion resistance. This is pertinent because the analyses of the behaviour of alloying elements in stainless steels can be extrapolated to WC-based composites.

In the future, in order to replace Co, partially or fully, with other elements, it is important to analyse the influence of these elements and their behaviour as binders for WC. In the case of Ni, it is added to stainless steel to improve the ductility and toughness of the steel, even with the increase in strength and hardness that it brings.

Ni is an interesting alternative binder because it has high wettability to WC, and a much superior performance regarding oxidation and corrosion, making WC-Ni cemented carbides much more relevant in corrosive media than WC-Co cemented carbides. However, the mechanical properties (hardness and strength) of WC–Ni cemented carbides are relatively inferior to those of WC–Co. The main disadvantage of Ni-based cemented carbides is their inferior mechanical strength. One reason is the higher stacking fault energy of Ni compared to Co (125 mJ/m^2 vs. 20 mJ/m^2), which makes Ni hardening only moderate. On the other hand, by combining Ni with Cr and Mo additions, and using it as a binder in WC-based composites, higher hardness numbers have been observed [8]. Another very relevant observation is that the size of the Co and Ni grains differs considerably. Co forms very large regions of single crystallographic orientation (up to 50 times larger than the average grain size of WC grains). Interestingly, Ni forms both large and small areas wherein no hcp structure is found. This is very relevant, because, usually, the smaller the grain size the higher the hardness of the material [8].

Importantly, the toxicity of Ni is on the same level as that of Co, which could, considering the new chemical legislation, limit further the development of pure Ni-based hard metals [1].

The use of Ni in WC-based alloys as substitutes for Co is mainly intended to take advantage of its behaviour against corrosion, similar to what happens in Ni-based alloys [9,10].

It is even possible that the total removal of Co is not favourable, and therefore, proceed to the partial use of Co, together with other alloying elements, such as Ni, Mo, Fe, and Cr [8].

As for Cr, it creates a passive superficial layer responsible for the high corrosion resistance of stainless steels.

A third element, Mo can be added to further increase corrosion resistance, in particular the pitting corrosion resistance, in combination with Cr. There is no consensus, however, on the mechanisms involved in the process. Ni-Cr-Mo is the core of corrosion-resistant Ni superalloys and is also famous for imparting superb corrosion resistance and high toughness [11-14]. The combination of these elements has proven to have a lot of relevant properties regarding high corrosion resistance in aggressive media and still possess high hardness and toughness [8]. It is possible that a similar combination could replace Co in WC-based composites. In order to achieve a partial or full replacement, it is important to analyze the influence of these elements and their behaviour as binders for WC.

The main objective of this work is to evaluate the mechanical and electrochemical behaviour of several WC-Ni-based composites in a comparative analysis of their performance.

This document is divided into 3 main parts. The first part, which relates to Chapter 2, provides a state-of-the-art overview of existing studies and tools in the areas addressed in the development of this dissertation. The other two parts define the main core of the thesis and are covered in Chapters 3 and 4.

In Chapter 3, the experimental part of this dissertation is explained succinctly. The solution used, the processes applied, its components and the methods used to conclude this work.

In Chapter 4, results and discussion are addressed and comparison and seriation of the data were made.

Finally, in chapter 5, there is an overall conclusion of the work that has been done, and considerations are made. There is a theoretical proposal of the best alloys to use and suggestions and motivation for future work, derived from the results of this dissertation.

The natural curiosity of the human species and the motivation to innovate and develop new instruments and tools to make life easier, dates as far as pre-historic times, and nowadays is no different, just more refined. Every day, hundreds of ways to facilitate life are invented and discovered, and this will continue forever, as the search for knowledge will forever be infinite and the need to know and learn is intrinsic to humanity.

Chapter 2

2. State of the Art

The purpose of this chapter is to review existing studies in the areas covered in the development of this dissertation focusing on evaluating how the previously known and industrially used grades behave from the point of view of hardness, fracture toughness, corrosion, and wear resistance. Studies, where polarization, open circuit potential measurement and electrochemical impedance spectroscopy are performed, will be taken into consideration. Existing studies and papers regarding WC-Co, WC-Ni, WC-Ni-Co WC-Fe-Co-Ni, WC-Ni-Cr-Mo and WC-Ni-Cr-Co-Mo alloys and stainless steels (with Ni-Cr-Mo) will be evaluated and taken into consideration. Next, some concepts of interest in the context of this dissertation may be taken into consideration as well. Finally, existing solutions for good corrosion resistance alloys for seawater applications may also be taken into consideration.

To adjust the microstructure and mechanical properties of cemented carbides there is one step that is of most importance, the sintering step. Densification takes place during the sintering, to obtain a pore-free microstructure and the final dimensions of the component. Liquid phase sintering is the industry basis for producing cemented carbides.

As reported in [15,16] there are four major steps during the sintering process.

In the first step, the binder and the impurities are degassed, and the oxides are reduced, both contributing to the shrinkage of the cemented carbide.

In the second step, the temperature starts to rise, and solid-state sintering begins to occur. The binder phase begins to wet the WC grains and dissolution starts to occur. Transport of material takes place by solid-state diffusion and bulk transport. As the temperature increases porosity increases and the material that was dissolved in the binder metal will start to re-precipitate on undissolved grains. The particles are re-arranged leading to densification enhancements, followed by further shrinkage.

In the third step, as the melting temperature is achieved, which is around 1300 to 1400 ºC for a WC-based alloy saturated in carbon, liquid phase sintering starts to take place. The solubility product controls the grain dissolution in the binder phase until its saturation. The larger grains that are not dissolved grow at the expense of the smaller ones because they dissolve preferentially. This Ostwald Ripening (phenomena in which smaller particles in solution dissolve and deposit on larger particles to reach a more thermodynamically stable state wherein the surface to area ratio is minimized) process leads to coarsening of WC grains but on the other hand, it aids in the completion of densification.

In the fourth and last step, the cooling of the material, the binder phase solidifies. Some re-precipitation takes place in the step originating further coarsening. Typically, the sintering process occurs in sintering furnaces with strictly controlled

parameters (temperature, atmosphere, pressure, heating/cooling rates and sintering times).

Microwave sintering or spark plasma sintering are two examples of processes that have already been explored to try and produce cemented carbides, but they are not established in the industry.

During the full cycle of sintering, it is of most importance to control the sintering atmosphere. This is necessary to reduce the pressing binder (debinding), lessen the oxide scales of the metal binder and carbides particles (vacuum step) and avoid binder transport or surface decarburization during the liquid sintering step (controlled gas mixture) [36].

2.1 Microstructural characterization

Some of the main properties known to affect the overall performance of WC-based composites are WC particle size, distribution, and the amount of binder present in the alloy.

It has been proven that the addition of Cr to WC-Co and WC-Ni-based alloys increases the corrosion resistance of these alloys [17-20]. On the other hand, Cr has a very increased affinity for carbon, which cancels out the possibility of adding large amounts of Cr to the alloy due to a decrease in general performance [21]. This is a fact because by adding large quantities of Cr the material densification decreases by a significant amount [22,23].

From the literature, Cr content should be kept within an ideal range, so that the advantages of corrosion resistance can be achieved without damaging the overall mechanical performance.

Interestingly, correlated works revealed that the presence of 0.6 wt% Mo reduces composites densification, inhibits grain growth [24,25], and increases the corrosion resistance of WC-Ni-Cr-Mo composites in acidic chloride and sulphate-based solutions, without hindering the mechanical properties [9,10,26,27].

It is not known the exact mechanism by which Mo increases the resistance to pitting corrosion. However, several ideas have been proposed to explain the effect of Mo presence in stainless steels. Repassivation enhancement and higher resistance to the breaking down of the passive film present on the surface [28,29], and the reduction of the dissolution rate of the bare metal [30,31], are some of the mechanisms proposed.

When in the presence of a sulfate media, Mo forms a MoS_2 protective film enhancing the corrosion resistance even further [32].

Both N. Lin *et al.* and Qiankun Zhang *et al.* [33,34] reported a significant increase in corrosion resistance for chloride medium, for 1 wt% and 1 and 2 wt%, respectively.

The influence of Mo is extensively exemplified in stainless steels [35-37]. On the other hand, this is not the case for WC-based composites, which are still severely uncharted territory. Despite its overwhelming good qualities, the addition of Mo also

presents some problems. Some WC composites containing Mo, presented a significant loss of fracture toughness, which can quickly transform into a harmful attribute [38].

This work will consider the performance of WC-Co in tribocorrosion situations and the evaluation of its replacement by other elements, such as Ni, Cr and Mo. It also aims to evaluate the hardness, fracture toughness (K_{1c}) and corrosion resistance of the alloys under analysis.

As was observed by Santos *et al*. [9] and can be observed in Fig. 1 and Fig. 2, the addition of 0.6% of Mo can hinder WC grain growth. This was concluded because the grain sizes were measured and a greater number of grains with sizes inferior to 0.8 μm were observed when compared to the samples with 0.1% and 0.4% Mo. The samples with 0.1% and 0.4% Mo did not represent any statistically significant effect on the grain size distribution. This leads to the conclusion that Mo additions are mostly beneficial above 0.6%. Further studies with increasing Mo quantities could prove enlightening regarding this matter. In Santos *et al.'s* work [9], it is also noted that there is an apparent decrease in fracture toughness < 4%, and a minor increase in hardness, about 5%. It is explained that this is due to having a smaller WC grain size because of the hindering in grain growth the presence of Mo induces. Typically, smaller grain size in metals indicates a higher hardness. The increase in hardness is also connected to the solid solution strengthening effect promoted by the presence of Mo. In this article it was concluded that Mo presented visible benefits in contents of 0.6 wt% for improved corrosion resistance in WC-Ni-Cr-based composites, thus enhancing the anodic active-passive transition in chloride medium and ensuring the passivated state in a sulphate solution. This provides the base ground for one of the main focuses of this dissertation, concluding if the addition of Mo will prove effective in replacing Co as part of the binder for WC-based composites [9].

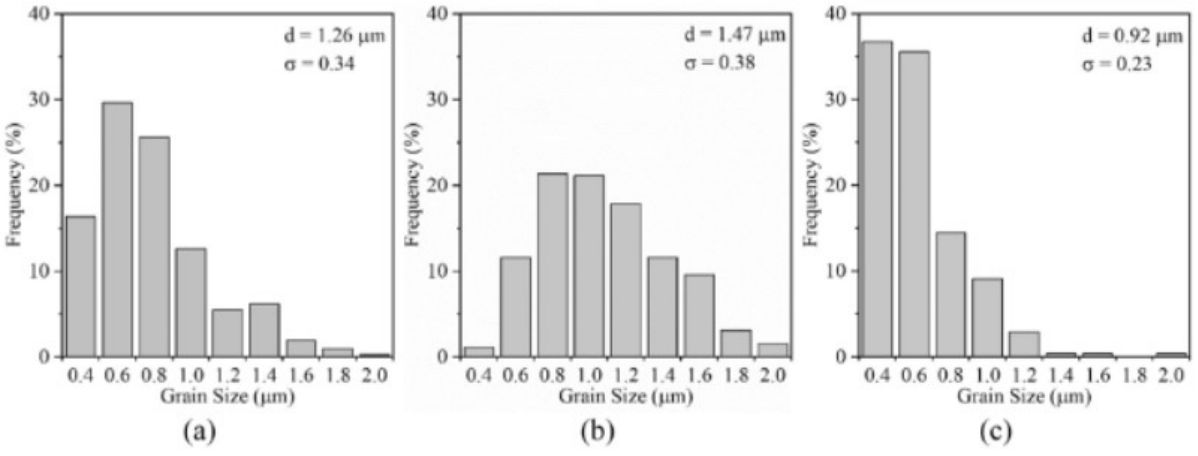

Figure 1 - Grain size distributions for Mo-1 (a), Mo-4 (b) and Mo-6 (c) [9].

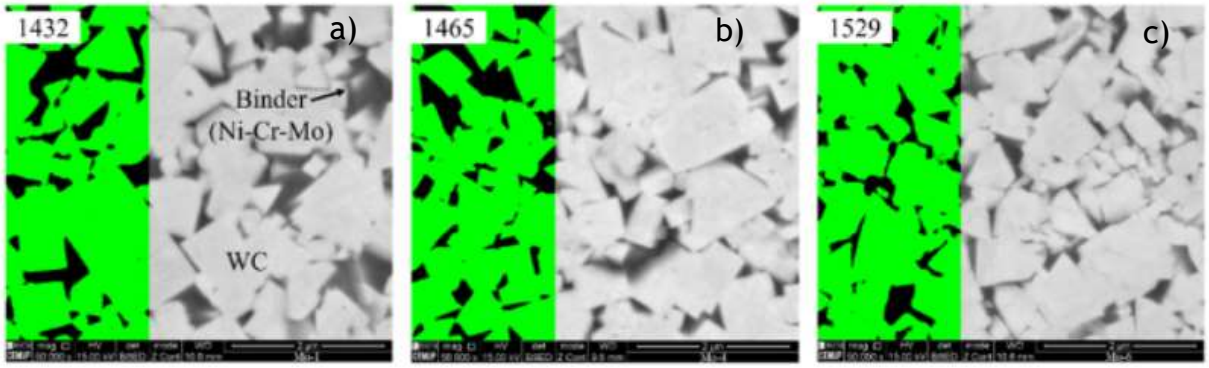

Figure 2 - SEM microstructures of WC-Ni-Cr-Mo, their respective binary images highlighting WC (green) and binder (black) and Vickers hardness for 0.1 (a), 0.4 (b) and 0.6 wt% Mo (c) specimens [9].

In another work carried out by Santos *et al*. [10] instead of varying the content of Mo, what was varied was the content of Cr, to study its effects on corrosion-resistant WC-based alloys. WC particle size distributions for variations of Cr of 1.1%, 1.3% and 1.8% revealed identical average grain sizes for all the specimens. In the case of the sample with 1.1% of Cr, it had a broader grain size distribution. All the above can be observed in Fig 3. The area fraction for the samples was measured using images taken on SEM micrographs (Fig. 4) and used as an indicator of the material's volume fraction.

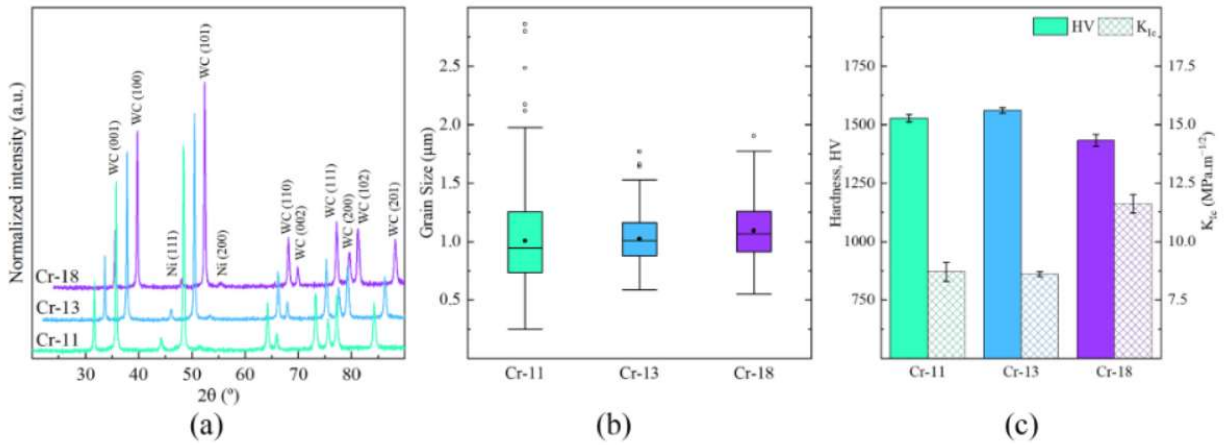

Figure 3 - XRD patterns (a), box plots for grain size distributions (b), and hardness and fracture toughness (c) for the three specimens [10].

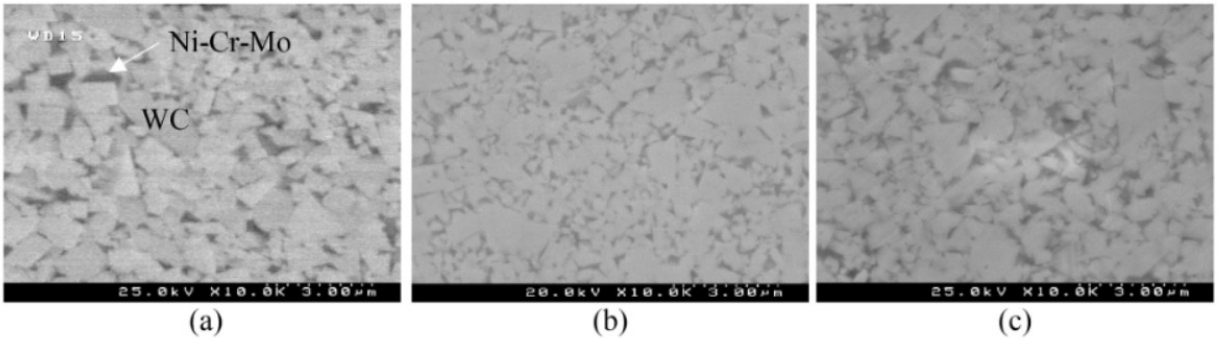

Figure 4 - SEM microstructures of WC-Ni-Cr-Mo for 1.1 (a), 1.3 (b) and 1.8 wt% Cr (c)

In Ferro Rocha *et al.'s* work [8] , the microstructure of WC-based composites was analysed by SEM, after being polished and etched with Murakami's solution. The microstructures encountered by Ferro Rocha *et al.* [8] are homogeneous, with the WC grains well dispersed in the binder, and almost no porosity. Through the SEM images visible in Fig. 5, the authors conclude that the carbides Cr_3C_2 and Mo_2C are completely dissolved in the binder phase without any problems regarding secondary phases. No free carbon or η-phase was encountered.

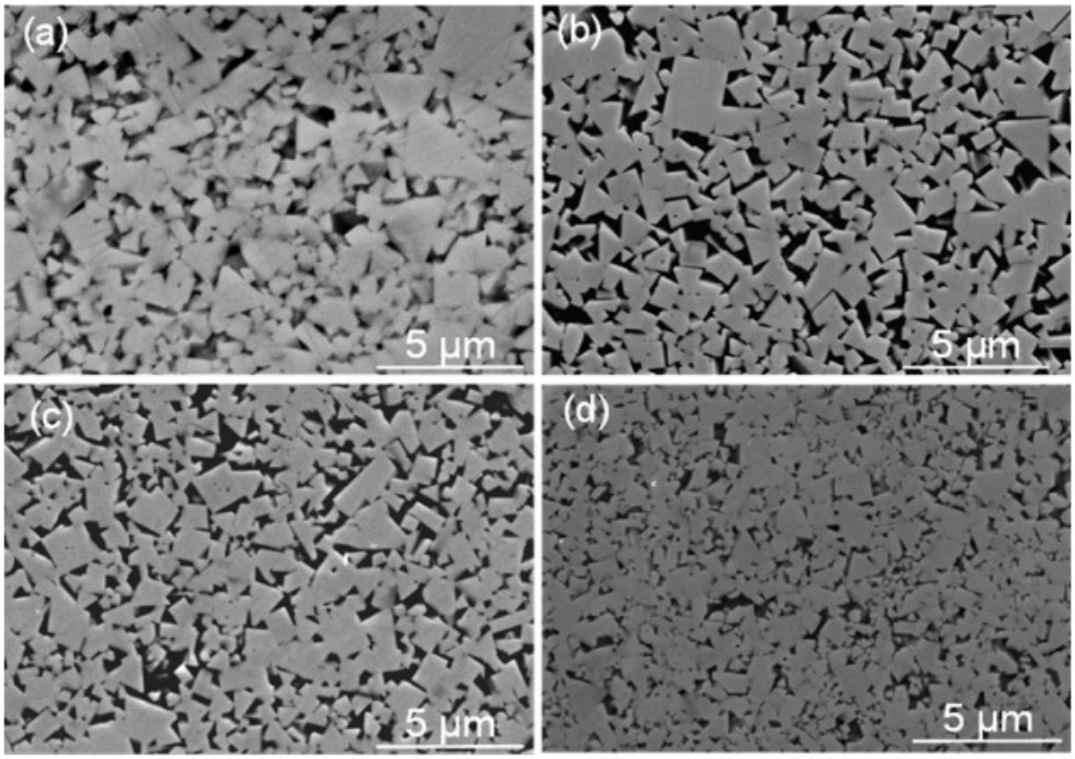

Figure 5 - SEM images of polished surfaces etched with Murakami's solution: (a) WC-Co; (b) WC-Fe-Co-Ni; (c) WC-Ni-Cr-Co-Mo and (d) WC-Ni-Cr-Mo [8].

The XRD spectra presented in Fig. 6, and the article by Ferro Rocha *et al.* [8], support the microstructural analysis since the WC phase is present in every spectrum along with the binder-related phases. The elements in a greater amount in each alloy are the only ones that give a peak small peak in the spectra, Fe (α) and Fe-Ni in Fe-Co-Ni, and Ni in Ni-Cr-Co-Mo and Ni-Cr-Mo. The rest of the metallic elements that are present in the alloys are dissolved in the matrix and do not give an individualised spectrum due to being integrated in its structure [8].

2.2. Mechanical Properties

Alternative composites, such as WC-Fe-Co-Ni, WC-Ni-Cr-Co-Mo and WC-Ni-Cr-Mo can achieve similar or even higher hardness than that of some typical commercial grades WC-Co-based alloys [8].

In Ferro Rocha *et al.*'s work [8], it was observed that the substitution of the Co by a Ni-Cr-Mo binder increased the hardness of the material, as can be seen in Table 1, but decreased the fracture toughness. The values of K_{1c} determined for all the analysed specimens were lower than for the WC-Co alloy, however, they are still inside the acceptable range for hardmetals. Depending on the application this can be a determining factor. On the other hand, the presence of Mo and Cr in both WC-Ni-Cr-Co-Mo and WC-Ni-Cr-Mo did not increase the porosity of the material and decreased the average size of the grains to half. This decrease was more noticeable in the case of WC-Ni-Cr-Mo and is related to the absence of Co in this sample, which is known to promote WC grain growth [8].

Table 1 - Physical and mechanical properties of all composites studied by A.M.F. Rocha *et al.* [8].

	Density[a] ($g\ cm^{-3}$)	G_{avg}[c] (μm)	Hardness (HV30)	K_{IC}[d] (MPa $m^{1/2}$)
WC-Co	14.30	1.00	1420 ± 19	14.3 ± 0.7
WC-FeCoNi	14.12	0.81	1369 ± 12	10.5 ± 0.3
WC-NiCrCoMo	14.21	0.75	1495 ± 18	9.5 ± 0.2
WC-NiCrMo	14.33	0.52	1577 ± 16	10.6 ± 0.2

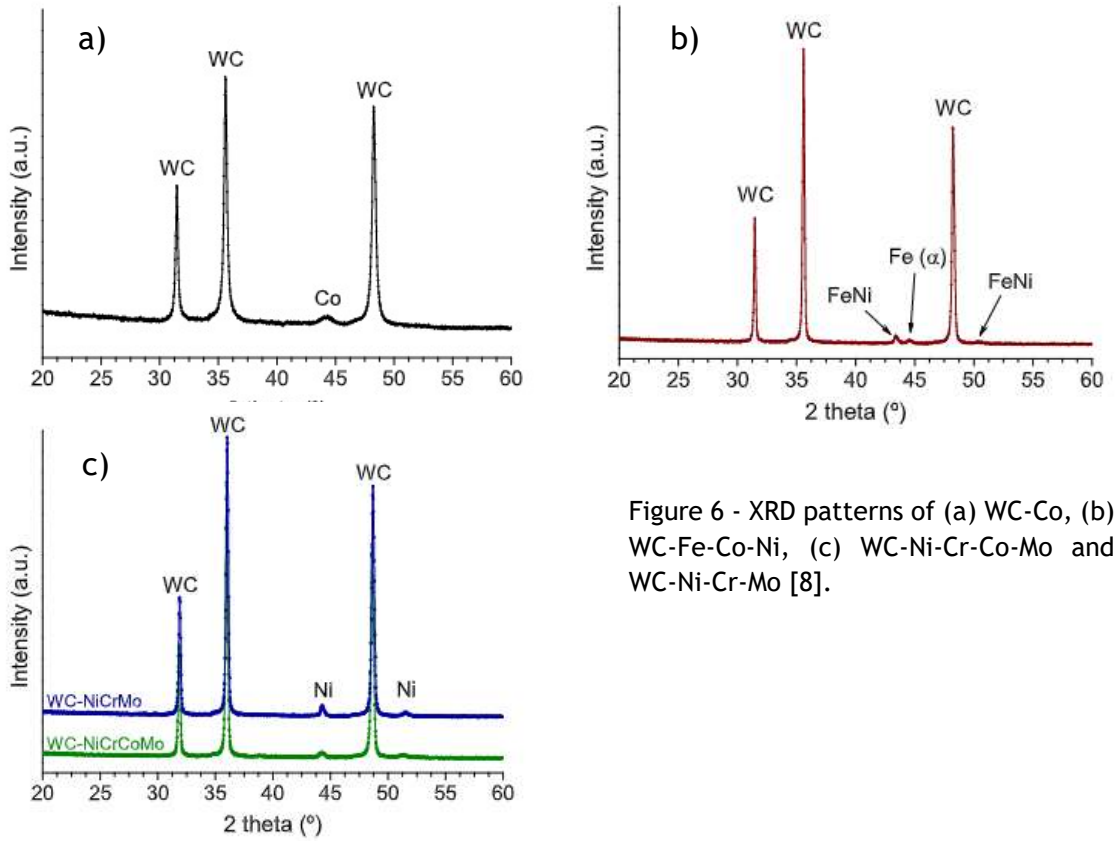

Figure 6 - XRD patterns of (a) WC-Co, (b) WC-Fe-Co-Ni, (c) WC-Ni-Cr-Co-Mo and WC-Ni-Cr-Mo [8].

In Santos, *et al.*'s work [10], when comparing the first two samples, 1.1 and 1.3 wt% of Cr, there was no pertinent impact on mechanical performance. On the other hand, when analysing and testing the sample with 1.8% of Cr, it shows a lower hardness and a higher fracture toughness, however, this was attributed to a lower WC volume fraction and a higher percentage of binder in the alloy [10].

2.3. Electrochemical Characterization - corrosion

In Santos, *et al.*'s work [10], all specimens were submitted to a routine of electrochemical experiments, consisting of surface preparation, surface cathodic cleaning set to 0.5 V vs. Ag/AgCl for 300 s, open circuit potential (OCP), E_{oc} measurement for 6 h vs. Ag/AgCl, electrochemical impedance spectroscopy (EIS) ranging from 100000 to 0.01 Hz (±15 mV rms vs. E_{oc}), conditioning at 0.6 V vs. Ag/AgCl for 300 s, followed by potentiodynamic polarization ranging from 0.6 to 1.0 V (at 1 mV/s).

It was proven through the experiments performed by Santos, *et al.* [10] that the addition of up to 12 wt% of Cr in the binder can provide increased corrosion resistance due to the active passivating film it generates in the alloy, all without decreasing the hardness. Lower contents of Cr (9.7wt%) also proved to have good performance in a sulfate solution media and only improved slightly for higher Cr contents.

The major corrosion resistance improvements were observed in chloride media, which is the media that displays higher aggressiveness towards the binders present in WC-based alloys. To guarantee good corrosion resistance it is recommended that the ratio between Cr and binder is kept above 11 wt%, because in the lower Cr content alloy, the development of an insulating barrier from the solution was not observed or a porous film was formed instead [10].

In another work carried out by Santos, *et al.* [9], the same routine was applied to 3 samples varying the wt% of Mo instead of Cr, being the only difference that the open circuit potential was performed for a total of 8 h instead of 6h, to have a more stable final potential value, and that the peak for the electrochemical impedance spectroscopy was 10 mV instead of 15 mV.

It was proven through the experiments performed, that chloride media are more aggressive to WC-based composites than sulphate media. Also, it was clear that the addition of 0.6 wt% enhanced the anodic active-passive transition in chloride medium and ensured the passivated state in a sulfate solution. These results proved that Ni-Cr-Mo is a very interesting candidate to replace Co as a binder for WC-based composites. A conclusion was also drawn regarding intermediate additions of 0.4 wt% Mo, appearing to be harmful, contributing to a small decrease in corrosion resistance [9].

Ferro Rocha *et al.* [8], performed some similar experiments on WC-Co, WC-Fe-Co-Ni, WC-Ni-Cr-Co-Mo, and WC-Ni-Cr-Mo specimens that prove relevant to this

dissertation. Ferro Rocha *et al*. [8], showed that for a 24h immersion in a 0.5 M NaCl solution, E_{ocp} values for the WC-Ni-Cr-Co-Mo and WC-Ni-Cr-Mo specimens were 400 mV more positive than for WC-Co and WC-Fe-Co-Ni, thus proving that these samples are indeed less susceptible to corrosion.

Regarding the polarization curves performed and analysed by Ferro Rocha *et al*. [8], Tafel extrapolation was used to determine the corrosion rates (i_{corr}) and the corrosion potential (E_{corr}). The lowest corrosion rates were obtained for WC-Ni-Cr-Mo and WC-Ni-Cr-Co-Mo (~ 0.2 and 0.6 $\mu A.cm^{-2}$, respectively) which are about one order of magnitude lower than for WC-Co and WC-Fe-Co-Ni.

Regarding the electrochemical impedance spectroscopy experiments performed by Ferro Rocha *et al* [8], the two composites with Ni-Cr-Mo present in the binder (WC-Ni-Cr-Co-Mo and WC-Ni-Cr-Mo) exhibited much higher impedance (nearly 10^6 $\Omega.cm^2$) with a capacitive response, typical of passive systems. In conclusion, in Ferro Rocha *et al*.'s work [8], signs of corrosion were observed in WC-Co (Fig. 7) and WC-Fe-Co-Ni since the first day of immersion while no traces of attack were observed in WC-Ni-Cr-Co-Mo and WC-Ni-Cr-Mo (Fig. 8) during the whole testing period.

WC-Fe-Co-Ni behaved similarly to WC-Co, presenting an insufficient corrosion resistance. On the other hand, WC-Ni-Cr-Co-Mo and WC-Ni-Cr-Mo revealed significantly higher corrosion resistance, proving them as good replacements for WC-Co in neutral and near-neutral chloride environments [8].

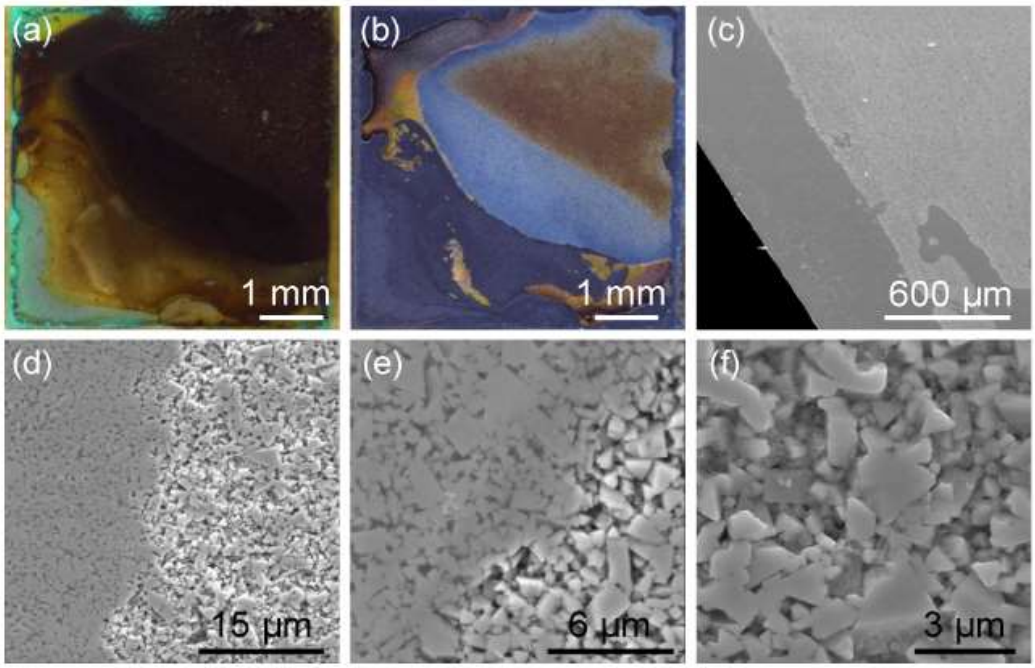

Figure 7 - Optical and SEM images of WC-Co after 2 weeks of immersion in 0.5 M NaCl. a) surface at the end of the testing; b) same area after removal of the loose corrosion products (flushing the surface with distilled water); c) interface between the tested area and the surface protected by the adhesive tape; d) magnification of the interface; e) detail of d); f) corroded area (lack of binder surrounding the WC particles) [8].

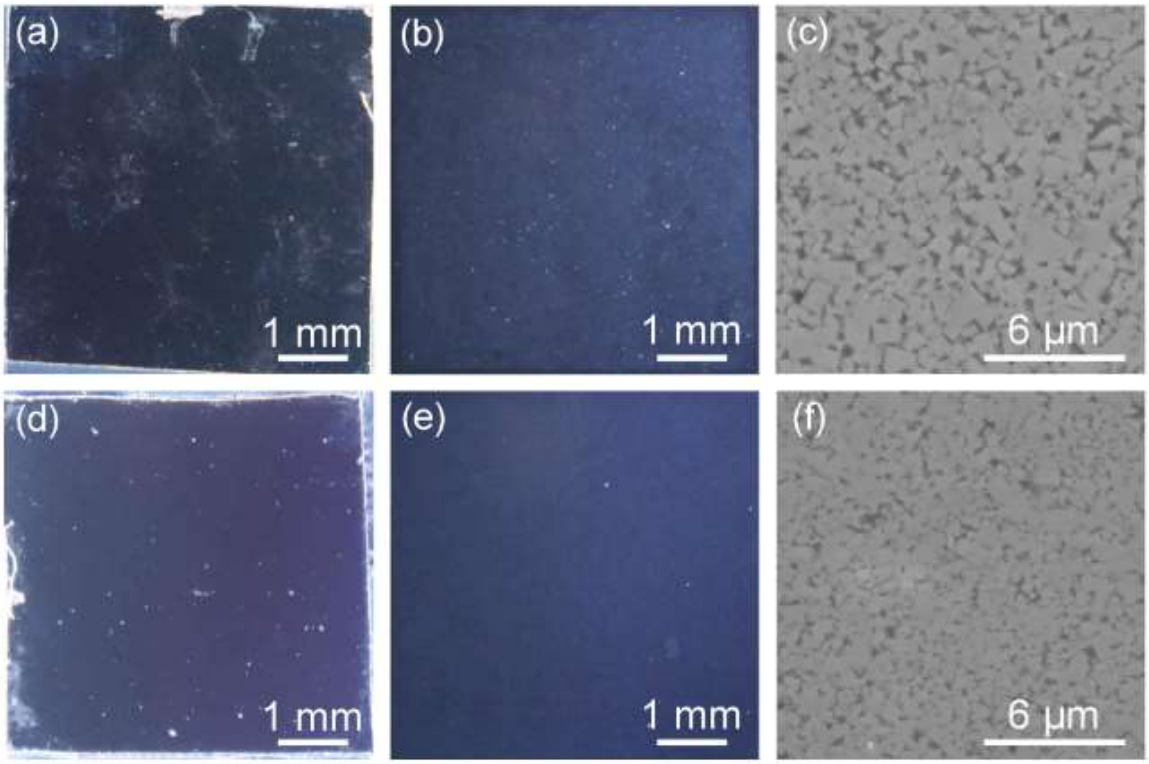

Figure 8 - Optical and SEM images of WC-NiCrCoMo (a–c) and WC-NiCrMo (d–f) after 2 weeks of immersion in 0.5 M NaCl: a) and d) surface of the samples just after testing; b) and e) same surfaces after flushing the surface with distilled water; c) and f) microscopic detail of the tested areas, showing no signs of corrosion [8].

2.4. Wear

In Boukantar *et al.*'s work [38], a comparison is done between WC-Co, WC-(Co-Ni), and WC-(Co-Ni-Cr)

The effect of mechanical wear by itself is taken into consideration. From the dry tribological tests performed, the coefficient of friction (COF) throughout the distance travelled is obtained. All three specimens had roughly the same friction curve, where the friction was strikingly smooth and low, with a steady-state COF of only ~0.06. For values this low, a very efficient lubrication process had to be operating during the dry tribological tests.

As seen in Fig. 9 and Fig. 10, the wear tracks are very narrow and very similar in size (width ~130 µm). According to Boukantar *et al.*, the explanation for such a thin wear track is the formation of an oxide tribolayer. These tribolayers form in situ during the tribological tests due to the frictional heating generated under the air atmosphere and are thinner in the inner region of the wear track because there, the greater cumulative wear, results in greater "polishing", thus providing a very efficient lubrication process allowing for such a low COF [38].

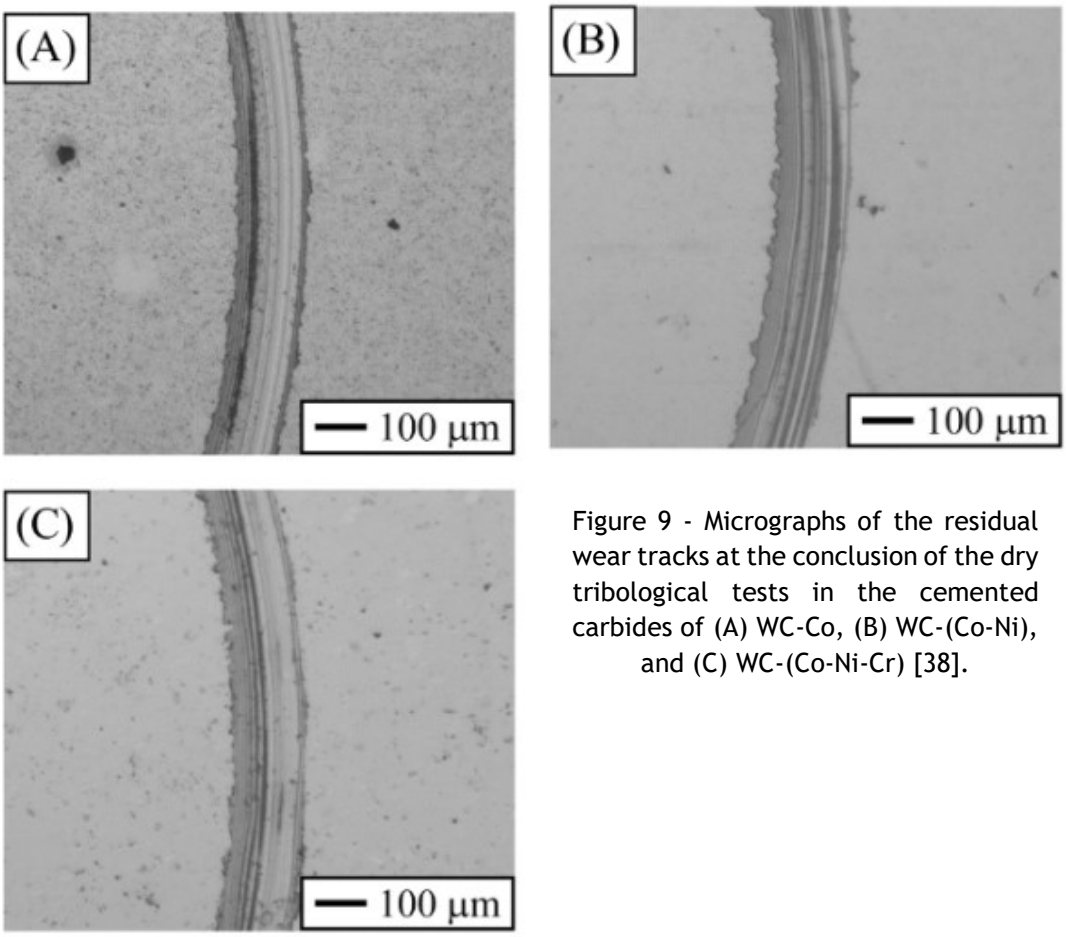

Figure 9 - Micrographs of the residual wear tracks at the conclusion of the dry tribological tests in the cemented carbides of (A) WC-Co, (B) WC-(Co-Ni), and (C) WC-(Co-Ni-Cr) [38].

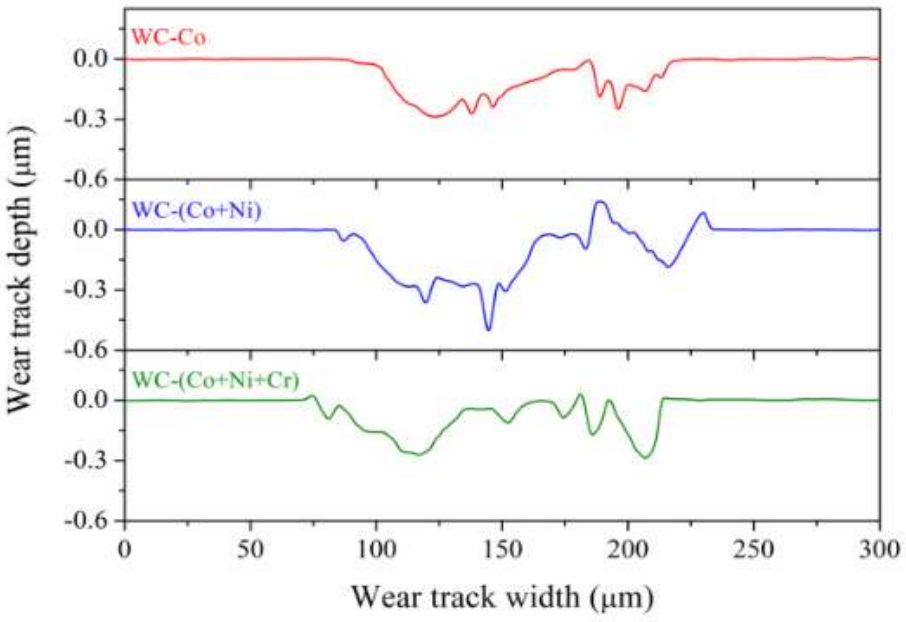

Figure 10 - Representative two-dimensional cross-sectional profile (i.e., depth vs width) obtained by OP of the residual wear tracks at the conclusion of the dry tribological tests in the cemented carbides of WC-Co, WC-(Co-Ni), and (C) WC-(Co-Ni-Cr), as indicated. These profiles are corrected by their baselines to avoid an inaccurate calculation of the worn volumes [38].

2.5. Tribocorrosion

As can be observed in the literature, according to Boukantar *et al*. it is shown that WC-Co, undergoes the most severe tribocorrosion, and separately the most intense corrosion and little mechanical wear, when compared to WC-Co-Ni and WC-Co-Ni-Cr, submitted to the exact same tribocorrosion tests, as can be seen in Fig. 11 and Fig 12.

WC-Co-Ni undergoes moderate tribocorrosion, and separately modest corrosion and little mechanical wear and WC-Co-Ni-Cr undergoes only slight tribocorrosion, and separately almost negligible corrosion and very little mechanical wear (Fig. 11 and Fig 12) [38].

As is expected, WC-Co has poor corrosion resistance, leaving a lot of room for improvement by adding other elements that are more corrosion resistant. In this study, values for tribocorrosion were calculated, leading to the conclusion that WC-Co-Ni-Cr is about ~7 times more resistant to tribocorrosion than WC-Co-Ni and ~20 times more so than WC-Co, and that WC-Co-Ni was, in turn, 3 times more resistant to tribocorrosion than WC-Co. Thus, these results support the established axiom that, among the cemented carbides, those with Cr in the binder are the most adequate for applications where tribocorrosion resistance is a primary concern.

In the WC-Co tribocorrosion test, as the main consequence of the consequent material removal and the continued immersion in the corrosive media, the recently revealed surface is exposed again to corrosion. This is particularly relevant under the pin-on-disk geometry because the cemented carbide is subjected to intermittent mechanical contact, thus favouring the interaction between the corrosive liquid media and the newly revealed surface of the cemented carbide. This procedure leads to a phenomenon where the corrosion accelerates wear and wear accelerates corrosion, making tribocorrosion of the WC-Co cemented carbide very deleteriously.

Concerning the WC-Co-Ni and the WC-Co-Ni-Cr tribocorrosion test, the same event is not verified. Ni and Cr and nobler metals than Co.

Binders of Co-Ni-Cr are particularly appealing because with this combination Co offers the needed sinterability, Ni provides the desired ductility and oxidation/corrosion resistance, and Cr gives the sought-for greater hardness and even more improved oxidation/corrosion resistance [38].

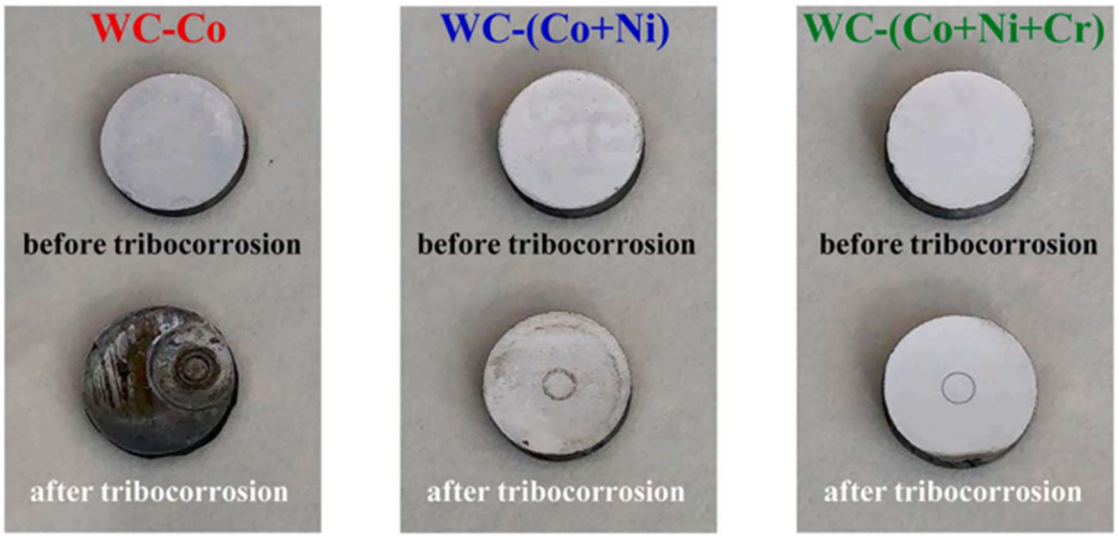

Figure 11 - Optical photograph of the cemented carbides of WC-Co, WC-(Co-Ni), and WC-(Co-Ni-Cr) taken both before and after the tribocorrosion tests in highly alkaline wet media (pH~13.65). The circle visible at the surface after the tribocorrosion tests is the corresponding residual wear track [38].

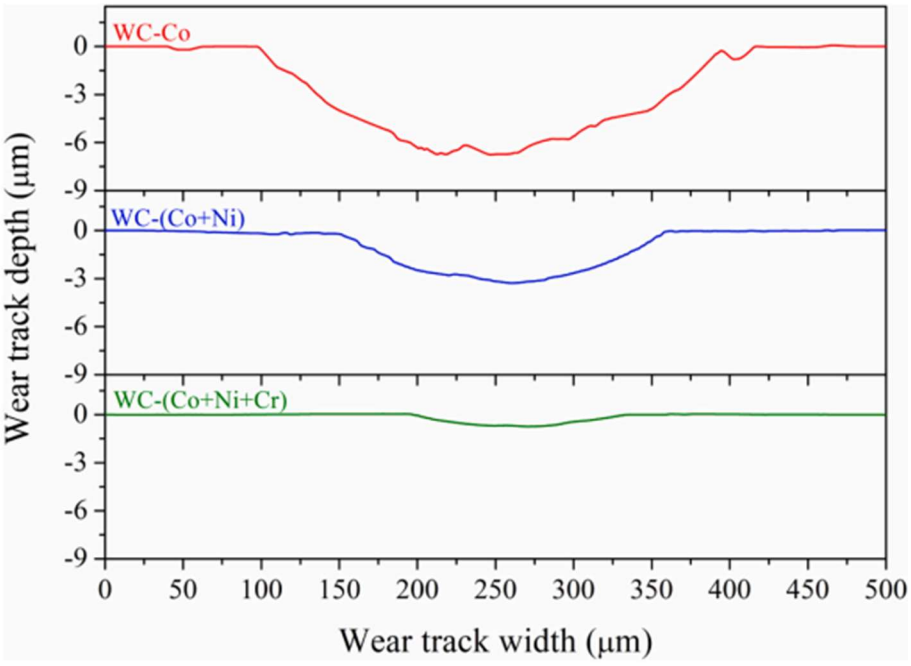

Figure 12 - Representative two-dimensional cross-sectional profiles of the residual wear tracks after the tribocorrosion tests in highly-alkaline wet medium (pH~13.65) in the cemented carbides of WC-Co, WC-(Co-Ni), and WC-(Co-Ni-Cr), as indicated [38].

3. Materials and Methods

3.1. Specimens Preparation

In total, this dissertation takes into consideration 8 different grades of cemented carbides, where 5 of them are the ones that constitute the main focus and are intended to be tested and investigated, to see if they are indeed viable. The other 2 are commercial grades.

The specimens were obtained from a mix of powders listed in Table 2 and 3. To produce the 5 specimens, the powders were weighted to produce 5 composite grades with increasing Mo (0.1 to 0.6 wt%, balanced by Ni), and Cr (1.1 to 1.8 wt%, balanced by Ni as well) content. To achieve a well-mixed composition, the powders are blended in ethanol in laboratory-scale ball-milling equipment for approximately 70 h. After this step, the entire mixture was dried out and compressed uniaxially to form small cylinders at 15 MPa. The cylinders went into a sintering process called sinter-HIP (sinter-HIP is a method of thermal consolidation for cemented carbide wherein the simultaneous application of heat and pressure fully consolidates the carbide) cycle up to 1440–1460 °C for a total of 90 min (sintering stage) and under 2 to 3 MPa of pressure in an Ar atmosphere [38].

Table 2 – Average Particle size

Powder	Average particle (μm)
WC	1.2
Ni	1-2
Cr3C2	1
Mo2C	1.6

Table 3 - Powders used to produce the specimens and their theoretical compositions, in wt%

Specimen name	WC	Ni	Cr	Mo	Co
M1	90	8.8	1.1	0.1	
M4C11	90	8.5	1.1	0.4	
M6	90	8.3	1.1	0.6	
M4C11	90	8.5	1.1	0.4	
C13	90	8.3	1.3	0.4	
C18	88.8	9.0	1.8	0.4	
WC-Ni-Co-Cr-Mo	----------	----------	----------	----------	----------
WC-Ni-Cr	91.2	8	0.8		
WC-Co	90				10

3.2. Chemical, mechanical, and microstructural characterization

The specimens started off by being grounded on a 54 μm diamond-coated disk, followed by an 18 μm one, at 300rpm. They were then polished to a mirror-like surface using a cloth with a 1 μm diamond suspension at 150rpm. The specimens were then rinsed in distilled water and dried at room temperature using soft paper. Subsequently, the specimens were analysed by SEM (FEI Quanta 450) and images were taken.

To determine the average hardness of each specimen, the Vickers method recommended by ISO 6507-1 (EMCO-TEST Dura Vision 20) with a load of 30 kg and a total of 5 indentations per specimen was utilized. To calculate fracture toughness (K_{Ic}), the Palmqvist method, which is based on hardness indentations, was used. This method was used in previous works for WC-Co, WC-Fe-Co-Ni, WC-Ni-Cr-Co-Mo and WC-Ni-Cr-Mo composites [8-10].

The K_{1c} is defined by Eq. (1), where A is 0.0028, H is the hardness in N/mm^2, P is the applied load in N and li is the crack length at each tip of the indentation, as can be seen in Fig. 13.

Volume fraction was calculated on ImageJ from SEM images by measuring the area fraction [8-10,41].

$$K_{IC} = A\sqrt{H}\sqrt{\frac{P}{\sum_{i=1}^{4} l_i}} \quad (1)$$

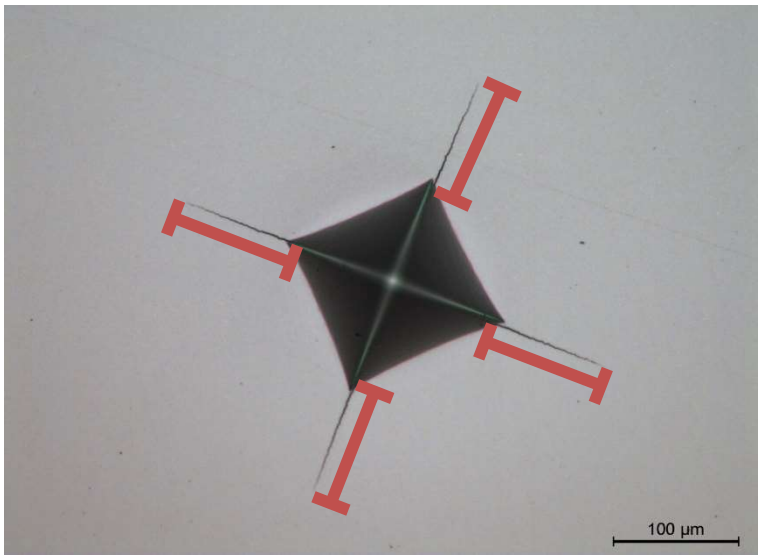

Figure 13 – Representation of how the li was measured in order to calculate K_{1c} for each of the identations

3.3. Electrochemical testing

One alkaline medium was used to simulate ocean water (designation D1141 – 98). This solution simulates the major effects of seawater corrosion on metals. This is particularly relevant due to the main developments and continuous new uses of hard metals in the gas, oil, and petrochemical industries, where ocean drilling is required, and corrosion wears the materials at an increased rate.

This practice provides two stock solutions, each relatively concentrated but stable in storage. For the preparation of synthetic seawater, aliquots of the two stock solutions with added salt are combined in a larger volume.

In designation D1141 – 98 it indicates how to produce 10 l of synthetic sea water and 7 l of each of the stock solutions. In Tables 4 and 5, the quantity of the salts needed to produce 7 l of the stock solution 1 and 2 and their concentration is specified.

In this dissertation, only 1L was needed to conclude all the experiments, so all the quantities were reduced to only produce this quantity. For stock solution 1, 20 mL were needed and for stock solution 2, only 10 mL, but to ensure that the error was minimal and to have the possibility to produce more synthetic seawater if needed, 100 mL were produced of each of the stock solutions.

Some of the reagents that were utilised, were somewhat different from the ones specified in the norm, which means some calculations had to be made to compensate for the reagent being more hydrated and not in the form specified by the norm.

To produce 100 mL of the first stock solution, all quantities were divided by 70 except for $CaCl_2$ (anhydrous). For this salt the following calculations were made, 5.794 g were needed, which means, 0.0522 mol was needed. To obtain this number of mols, through the rule of three we can easily conclude that 7.675 g of $CaCl_2 \cdot 2H_2O$ has the same number of mols as 5.794g of $CaCl_2$.

Table 4 – Quantity of the salts needed to produce 100 mL of the stock solution 1 and its concentration

$MgCl_2 \cdot 6H_2O$	3889.0 g	555.6 g/l
$CaCl_2$ (anhydrous)	405.6 g	57.9 g/l
$SrCl_2 \cdot 6H_2O$	14.8 g	2.1 g/l)

Table 5 – Quantity of the salts needed to produce 7L of the stock solution 2 and its concentration

KCl	486.2 g	69.5 g/l
$NaHCO_3$	140.7 g	20.1 g/l
KBr	70.4 g	10.0 g/l
H_3BO_3	19.0 g	2.7 g/l
NaF	2.1 g	0.3 g/l

In Tables 6 and 7, the actual quantities used to obtain the 100 mL of the stock solutions are specified.

Table 6 – Quantity of the salts needed to produce 100 mL of the stock solution 1 and its concentration

$MgCl_2 \cdot 6H_2O$	55.6 g	555.6 g/l
CaCl2·2H2O	7.7 g	7.7 g/l
$SrCl_2 \cdot 6H_2O$	0.2 g	2.1 g/l

Table 7 – Quantity of the salts needed to produce 100 mL of the stock solution 2 and its concentration

KCl	6.95 g	69.5 g/l
$NaHCO_3$	2.01 g	20.1 g/l
KBr	1.01 g	10.0 g/l
H_3BO_3	0.27 g	2.7 g/l
NaF	0.03 g	0.3 g/l

To produce the synthetic seawater itself, the salts in Table 8 were added to 800 mL of distilled water while stirring it manually until all the salts dissolve in the water. After that, 20 mL of stock solution 1 and 10 mL of stock solution 2 are added, all while stirring the mixture and until everything is well dissolved.

Table 8 – Quantity of the salts to be added to distilled water to produce 1 L of synthetic seawater

NaCl	24.536 g	24.536 g/l
Na2SO4	4.094 g	4.094 g/l

Finally, an adjustment of the pH to 8.2 was needed. To calibrate de pH probe a 2 points calibration was in need. Buffer solutions of 4 and 7 were used to guarantee the proper functioning of the probe. To adjust the pH to 8.2 a few droplets of NaOH were added to the solution while continuously measuring the pH with the pH probe.

To prepare the surfaces of the specimens for electrochemical testing, the preparation followed the exact same procedure used for chemical, mechanical, and microstructural characterization, as it was described in section 3.2. This procedure was repeated for each specimen prior to immersing it in the solution and starting off the electrochemical tests. The routine was prepared identically for all the specimens, as can be observed in Fig. 14 and Fig. 15. The white cord was connected to the reference electrode (Ag/AgCl (3 M KCl)), and the green was connected to the blue one, which was connected to the specimen via aluminium foil, the red one connected to the orange one which was connected to the counter electrode (Pt-coated Ti coil).

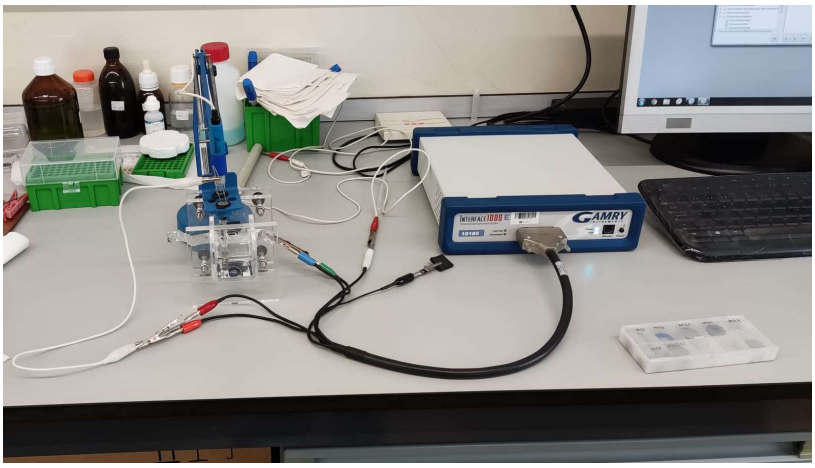

Figure 14 – Display of how the electrochemical tests were performed

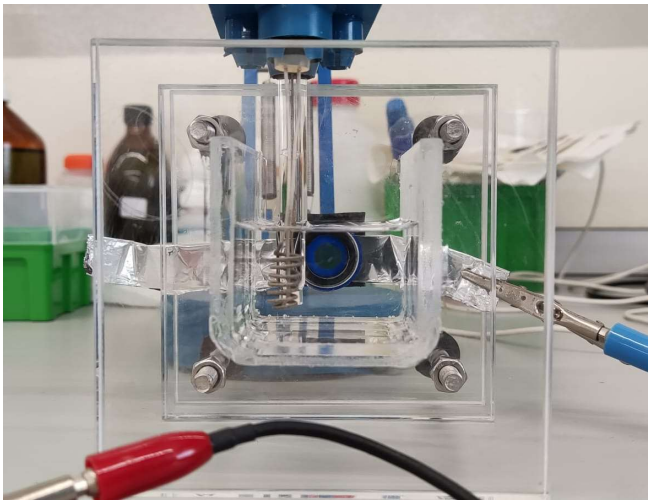

Figure 15 – Display of how the electrochemical tests were performed

As reference and counter electrodes, an Ag/AgCl (3 M KCl) and a Pt-coated Ti coil were used, respectively. A combination of electrochemical tests was carried out for each of the specimens listed in table 2 with a Gamry Interface 1000E potentiostat/galvanostat (Gamry Instruments, USA) and using Gamry Echem Analist software.

Each set was replicated at least two times, at room temperature, for each of the specimens, and a fresh portion of electrolyte was used in each procedure, starting approximately 10 min after surface preparation and 1 min after immersion (without stirring). The exposed surface area was 0.5 cm^2.

Each routine was constituted by three different tests. The routine started with an open circuit potential (OCP). This test measures the potential established between the working electrode (the metallic surface to be studied) and the environment (synthetic seawater), with respect to a reference electrode (Ag/AgCl (3 M KCl)) that was placed in the electrolyte close to the working electrode. This test has four major parameters, total time, in seconds, sample period, also in seconds, stability (mV/s) and

sample area (cm^2). The second to last one, tells the system the definition of a stable potential. If the absolute value falls under the stability parameter, the Corrosion Potential experiment ends immediately, disregarding the total time parameter. This test was performed for all specimens for a total of 4 hours and with a sample period every second. The stability value was set to 0 so that the limiting factor was always the total time. The sample area was set to 0.5 cm^2, which was the area of the working electrode [8-10,39,40].

The second test was an electrochemical impedance spectroscopy (EIS). Within short testing times, EIS measurements provide reliable data, allowing for the prediction of the long-term performance of the materials. This test applies a sinusoidal potential or a sinusoidal current to an electrochemical system and a corresponding sinusoidal current or a sinusoidal potential is measured. In this dissertation, a sinusoidal potential was applied, and a corresponding sinusoidal current was measured, this is what is referred to as a potentiostatic EIS. This type of EIS acquires an impedance spectrum over a range of frequencies. The input sinusoidal potential applied has several attributes. Firstly, it is time-dependent, which means the potential will fluctuate as a function of time. It also has an amplitude, which represents how big the applied potential is and has an angular frequency, which is a measure of how often the signal oscillates. The correspondent output sinusoidal current that is measured has the same attributes, it is time dependant, it has an amplitude, and it also possesses the same angular frequency as the input sinusoidal potential. However, the output sinusoidal current may be offset from that of the input sinusoidal potential. This offset is known as a phase shift or a phase angle. A complete electrochemical impedance spectroscopy experiment will consist of applying a sinusoidal potential centred around a potential set point at multiple frequencies. This set point was provided by the previous experiment, the open circuit potential. The correspondent output sinusoidal current is then measured at all these different frequencies creating a spectrum. These measurements generate two plots, denominated Bode and Nyquist plots. By a combination of these two plots and fitting them to an electrical equivalent circuit and modelling, it creates the ability to get a lot of qualitative and quantitative information about the electrochemical system. The electrical equivalent circuit that was used to represent the experiment is shown in Figure 16. In the model, 5 components are present, R.E. (reference electrode), Rsol (solution resistor), Rp (electrode resistor), W.E. (working electrode), Y0 (capacitance parameter) and a (deviation that the interface between solid and liquid have relatively to perfect condenser) [8-10,41].

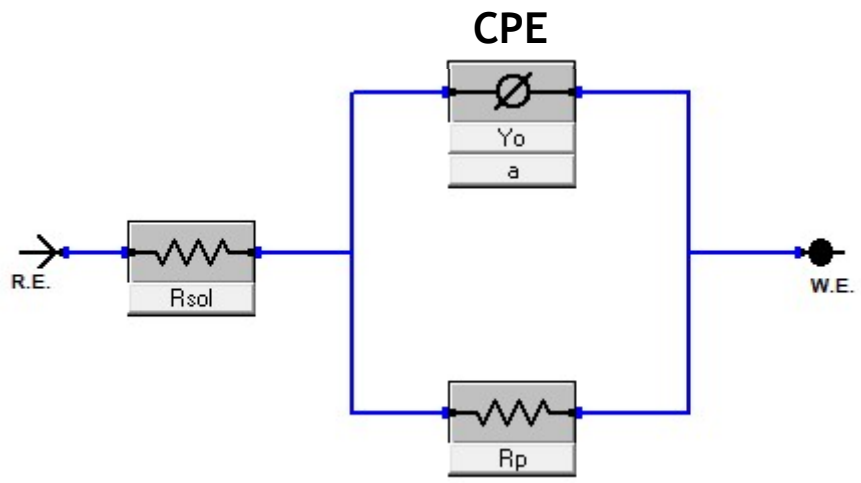

Figure 16 – Display of the electrical equivalent circuit models used for fitting EIS data

To start the experiment some parameters must be set, mainly the initial frequency and the final frequency. These were set to 100000 Hz and 0.01 Hz.

Following the Potentiostatic EIS came the cyclic voltammetry (CV). This experiment is a useful technique for extracting qualitative data from an electrochemical reaction. It is an electroanalytical chemistry technique where a potentiostat applies a triangular potential waveform to an electrochemical system and the resulting current is measured. The measured current is a function of time, although, the software plots it as a function of the applied potential, thus providing a cyclic voltammogram. Through this type of experiment, it is possible to conclude what is the corrosion potential (E_{corr}) for a given material and calculate the corrosion current (I_{corr}).

To do this, and in order to observe the graphics more easily, the Y-axis is converted to a logarithmic scale. This results in a transformation of the plot displayed and permits the observation of the corrosion potential. It is the lowest coordinate on the Y-axis. In the immediate surroundings of the lowest value current peaks, two linear zones allow the calculation of the corrosion current for a given material by drawing an imaginary line in the plot. To do this, plotting of the coordinates that form this imaginary line is made in Microsoft Excel and a tendency line is used to approximate the section. The equation of the tendency line is then used to calculate the E_{corr}, thus so having coordinates for both the corrosion current (E_{corr}, Y-axis) and for the corrosion potential (I_{corr}, X-axis). To start the experiment some parameters must be set as well, initial potential (initial E (V)), which was set to -0.5 V, scan limit 1 and scan limit 2, which were set to 1 and 0.95 V, respectively, and final potential (final E (V)), which was also set to 0.95 V, scan rate (mV/s), this being set to 1 meaning that every second the potential would increase by 1 mV. The sample area was also set to 0.5 cm^2 [8-10,42].

4. Results and discussion

4.1. Chemical and microstructural characterization

The volume fraction, size, and dispersion throughout the matrix of the reinforcement in a typical metal matrix composite are deeply tied with its mechanical properties and performance.

In Fig. 17 the WC particles are surrounded by a metallic binder of Ni, Cr and Mo and in Fig. 18 different binders are present (Ni, Co, Cr and Mo). Samples WC-Co and WC-Ni-Cr-Co-Mo function as comparisons to the principal 6 grades that are being evaluated in this work.

The WC grains appear as lighter, almost white areas, embedded in the binder phase (darker areas). The WC grains are very well dispersed in the binder and the microstructures are homogeneous.

The microstructure of each of the eight composites studied after polishing is presented in Fig. 17 and Fig. 18. The composites studied in this work display WC particles of slightly different sizes surrounded by a metallic phase consisting of Ni, Cr and Mo.

The volume fraction of the binder was estimated by measuring each of the specimen's area percentages on images taken with SEM. A total area of about 560 μm^2 was analysed for each specimen, and through software ImageJ, values between 17.3% and 20.5% were obtained, as can be observed in Table 9.

Table 9 – Binder volume fraction deduced from area fraction calculation on ImageJ

	M1	M4C11	M6	C13	C18	WC-Ni-Co-Cr-Mo	WC-Ni-Cr	WC-Co
Volume fraction	19.1	19.9	19.3	20.3	20.5	17.5	17.3	19.4

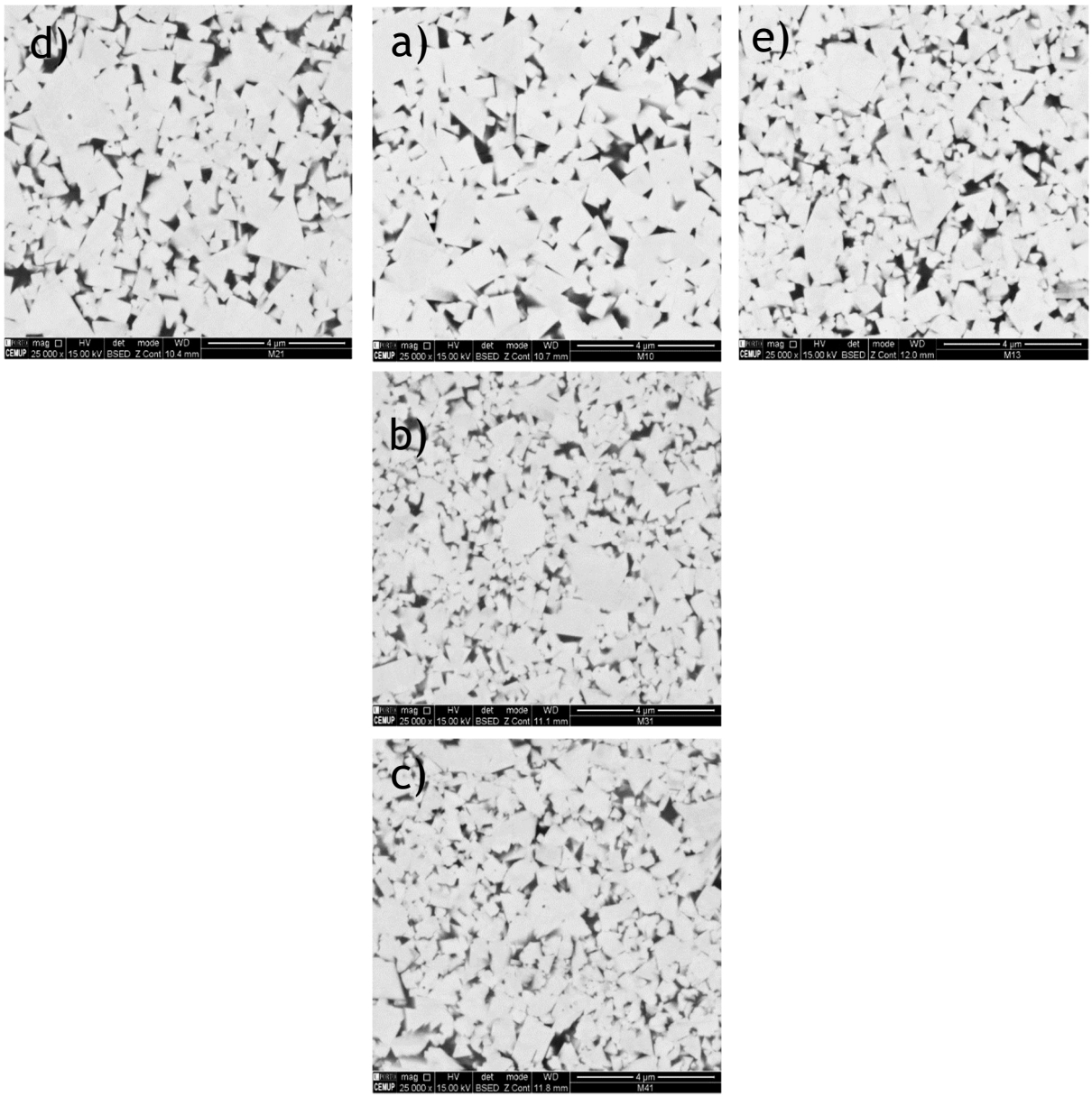

Figure 17 - SEM microstructures of WC-Ni-Cr-Mo for 1.1 (a), 1.3 (b), 1.8 wt% Cr (c) and 0.1 (d), 0.4 (a) and 0.6 wt% Mo

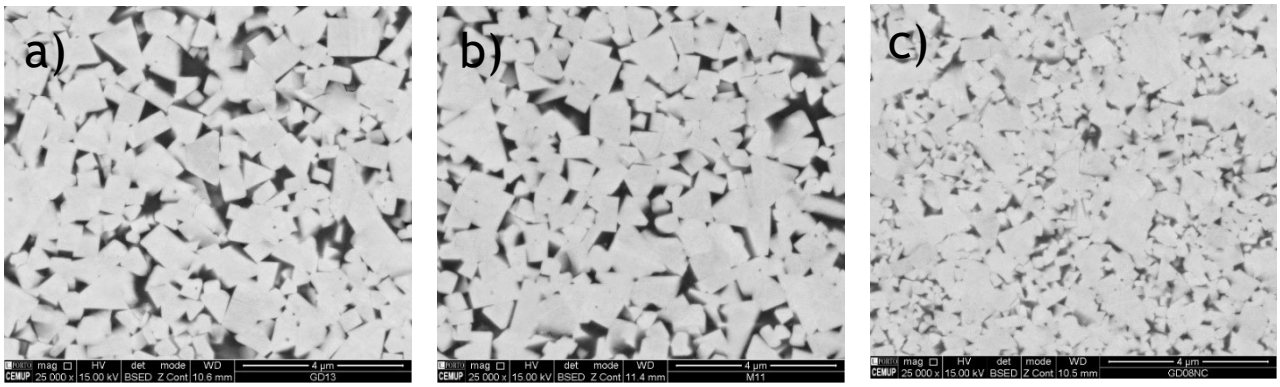

Figure 18 - SEM microstructures of WC-Co (a), WC-Ni-Co-Cr-Mo b) and WC-Ni-Cr c)

4.2. Mechanical characterization

The results of the mechanical testing, namely hardness and Palmqvist toughness, are presented in Table 10.

The lowest value of hardness was encountered for the M4C11 specimen, followed by WC-Ni-Co-Cr-Mo. On the other hand, the highest values were encountered in the WC-Ni-Cr specimen followed by the M6 and C13. M4C11 presented the highest K_{1C}, while the lowest value was from the C18 specimen. A noticeable increase can be observed when analysing the increase in Mo content. In the 0.1 (M1) and 0.4 (M4C11) wt% specimens, hardness was roughly the same, and both values are within the standard deviation. In the specimen with 0.6 wt% of Mo content, a notable increase is visible, around 100 HV30. This is owed to the fact that 0.6 wt% of Mo can inhibit grain growth, which can also be seen in Fig. 17.e). Also, the presence of Mo, originates solid solution strengthening effect, which can also be responsible for the higher hardness.

When analysing the Cr variation specimens there is also a noticeable increase. In this case, the two higher Cr-bearing specimens (C13 and C18) display the highest values for hardness while the M4C11 has lower values. Most probably, specimen C18 would have higher hardness values if Ni content was lower. The amount of binder present in this sample is 11.2 wt%, whilst the other two have 10 wt%, which makes it easily explainable why it has lower hardness values.

As is to be expected, as hardness rises, Palmqvist toughness decreases. This is not the exact case for all the specimens, as some of the specimens with higher hardness, i.e., the M6, still have high toughness.

When comparing the studied samples with the WC-Co specimen it is possible to observe that while keeping the same, or even higher hardness, all of the Mo variation specimens have higher fracture toughness. This increase goes to show that these alloys can easily substitute WC-Co in many applications where high hardness and high toughness are mandatory. When analysing the Cr content variation samples, a significant increase is observable in the C13 and the C18 specimen regarding hardness, when comparing them to the WC-Co specimen. On the other hand, toughness went down by a significant amount, which can be a limiting factor for some applications.

A comparison can also be drawn between the studied samples and the WC-Ni-Co-Cr-Mo and WC-Ni-Cr samples. These two have very similar fracture toughness, but very different hardness values. In the case of WC-Ni-Cr, this can easily be explained by analysing the amount of binder present in the specimen, roughly 8.8 wt%, so it is expectable for that grade to have a higher hardness. In the case of WC-Ni-Co-Cr-Mo, the lower hardness values can be attributed to low Mo contents and the presence of Co.

Table 10 – Values of Hardness (HV30) and Fracture Toughness (K_{1c} (MPa.$m^{1/2}$)) obtained for all the specimens tested

	Hardness HV30	K_{1c} (MPa$^{(1/2)}$)
M1	1472 ± 9	10.5 ± 0.2
M4C11	1461 ± 17	11.3 ± 0.4
M6	1577 ± 14	10.3 ± 0.3
C13	1580 ± 16	9.3 ± 0.2
C18	1541 ± 9	8.8 ± 0.2
WC-Ni-Co-Cr-Mo	1468 ± 9	9.3 ± 0.2
WC-Ni-Cr	1633 ± 10	9.0 ± 0.1
WC-Co	1484 ± 9	9.8 ± 0.2

4.3. Electrochemical evaluation

4.3.2. Open circuit potential measurements

The specimens were submerged in synthetic sea water roughly 10 min after preparing the surface. This was done to keep oxidation to a minimum and grant similar conditions for all the tested samples.

By observing Fig. 19, Fig. 20, and Fig. 21, it is clear that the open circuit potential (E_{oc}) increases very quickly for the first 30 to 60 minutes, in the direction of more anodic numbers for all the specimens, except for the WC-Co specimen.

In the Cr and Mo variation specimens, we can clearly see that the difference in the final potential is not much dissimilar between the different specimens. However, for all the specimens it is clear that at the end of the 4 hours of experiment, the potentials were still going up, even it being a very low value per unit of time.

By analysing Fig. 19 and Table 11, it becomes clear that the evolution of the E_{oc} has this behaviour due to the formation of an oxide film on the surface of the specimens. As the potential develops into more anodic values, this film grows thicker, which means it will make the specimen more insulated from the corrosive media

The difference in values between the three Mo content variation specimens is very small, but considering them, it is possible to rank them M1>M6>M4C11. The data that was obtained experimentally supports this ranking, however, it was to be expected that the higher the content of Mo, the more resistant to corrosion the specimen would be. This was not the case, as, for the intermediate value of Mo wt%, a lower OCP measurement was taken. This value should be in between the M1 and M6 specimen values, however, this result is in line with previous work for the same grade in acidic media [9], where the OCP measurements for the 0.4 wt% of Mo content were not in line with the evolution of the Mo content of the alloy. The reasons for such behaviour could not be identified. [8-10].

With the experimental data obtained it is possible to conclude that the passivating film is higher for the M6 and M1 specimen, as the E_{oc} was still going up in values at the time the experiment ended, whilst the M4C11 specimen did not display the same behaviour, as the E_{oc} was much more stabilised. A larger number of experiments per sample should be done to minimize average E_{oc} values uncertainty.

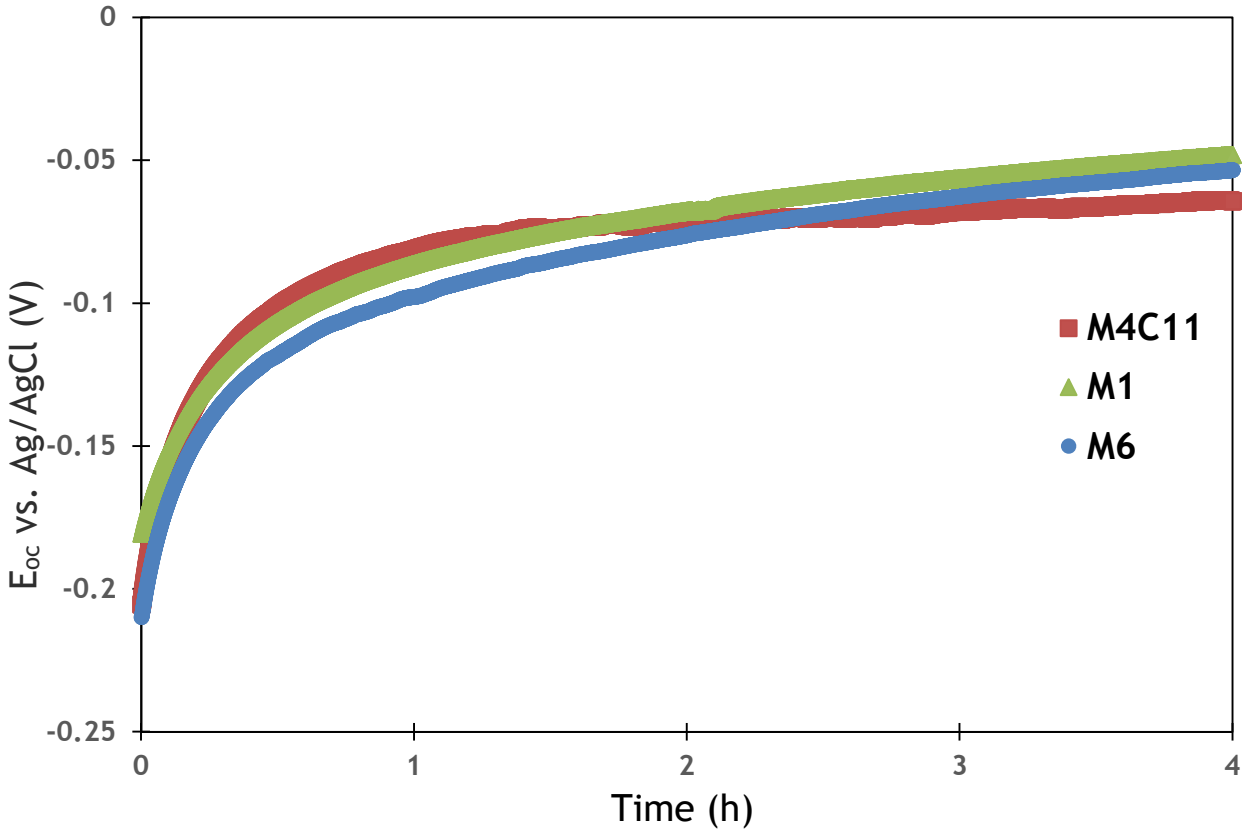

Figure 19 - Open circuit potential measurements for the variation of Mo wt% specimens after 4h of immersion

Table 11 – Average values for open circuit potentials for the variation of Mo specimens at the end of 4 h of immersion.

	E_{oc}(mV vs. Ag/AgCl)
M1	-47
M4C11	-50
M6	-53

When comparing with previous studies regarding composite grades with identical composition, there are some discrepancies. In Santos, *et al.*'s work, where two media were studied, one sulfate media and one chloride media.

In the sulfate media, the specimens behaved in the same way they behaved in the synthetic seawater. There is a formation of an oxide film on the surface of the specimens and as the potential develops into more anodic values, this film grows thicker, which means it will make the specimen more insulated from the corrosive media.

In the chloride media, the E_{oc} evolution was very steady, and the effect of the Mo variation did not seem to affect the open circuit potential values very much, although, there is a slight increase in the specimen with 0.6 wt% Mo. The potential increased only by a small amount between the beginning and the end of the experiments, suggesting that the film thickening that occurs in the media studied in this dissertation does not occur in a chloride media, or if it occurs, it is a much less intense one, i.e., a much less protective hydrated film. However, the synthetic seawater is indeed a chloride media, even though it has many more salts dissolved in them, which is somewhat contradictory. This phenomenon can be justified through the media´s pH, where in this dissertation the media is alkaline and in Santos *et al*. the media is acidic [2,18].

This supports the affirmation that these types of binders have a very desirable impact on the corrosion and tribocorrosion performance of these types of alloys.

By analysing Fig. 20 and Table 12, more than one conclusion can be drawn regarding the effect of the increasing Cr content on these types of alloys. When comparing these results with Santos, *et al*. previous work it is possible to conclude that 1.1 wt% of Cr still has a very desirable effect regarding corrosion resistance. Although significantly lower, the results were still very relevant. For the C13 and M4C11 samples the final open circuit potentials were -51 and -50 mV, showing that for 1.1 and 1.3 wt% of Cr content, the passivating layer is capable of providing good corrosion resistance. However, when considering the C18 specimen, it is clear that the addition of 1.8 wt% can effectively decrease corrosion susceptibility in these media, which follows in line with what was studied by Santos, *et al*. for both the chloride and the sulphate media [10].

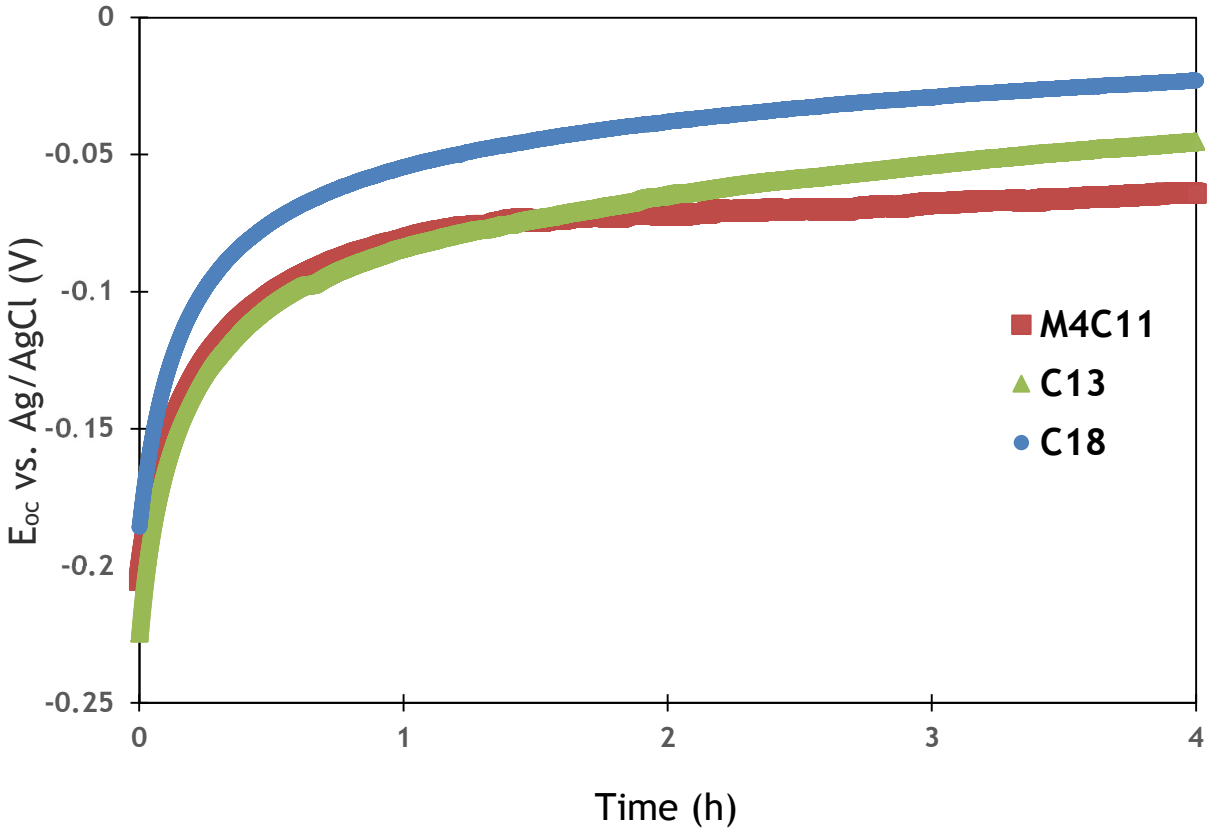

Figure 20 - Open circuit potential measurements for the variation of Cr wt% specimens after 4h of immersion.

Table 12 - Average values for pen circuit potentials for the variation of Cr specimens at the end of 4 h of immersion.

	E_{oc} (mV vs. Ag/AgCl)
M4C11	-50
C13	-51
C18	-27

Finally, when analyzing Fig. 21 and Table 13 it becomes clear that the WC-Co specimen has indeed a very low corrosion resistance. Contrary to all the other specimens, it peaks around -200 mV and then starts to go down in potential, stabilizing around -284 mV. Even without further experiments, it becomes clear that for chloride alkaline media (synthetic sea water) the WC-Co has a very poor performance. WC-Ni-Cr is a commercially used grade of hard metal and despite having a good performance in the substitute ocean water, the C18 specimen still had better performance. When analyzing the WC-Ni-Co-Cr-Mo specimen it is clear that the presence of Co has an unfavourable impact on the alloy.

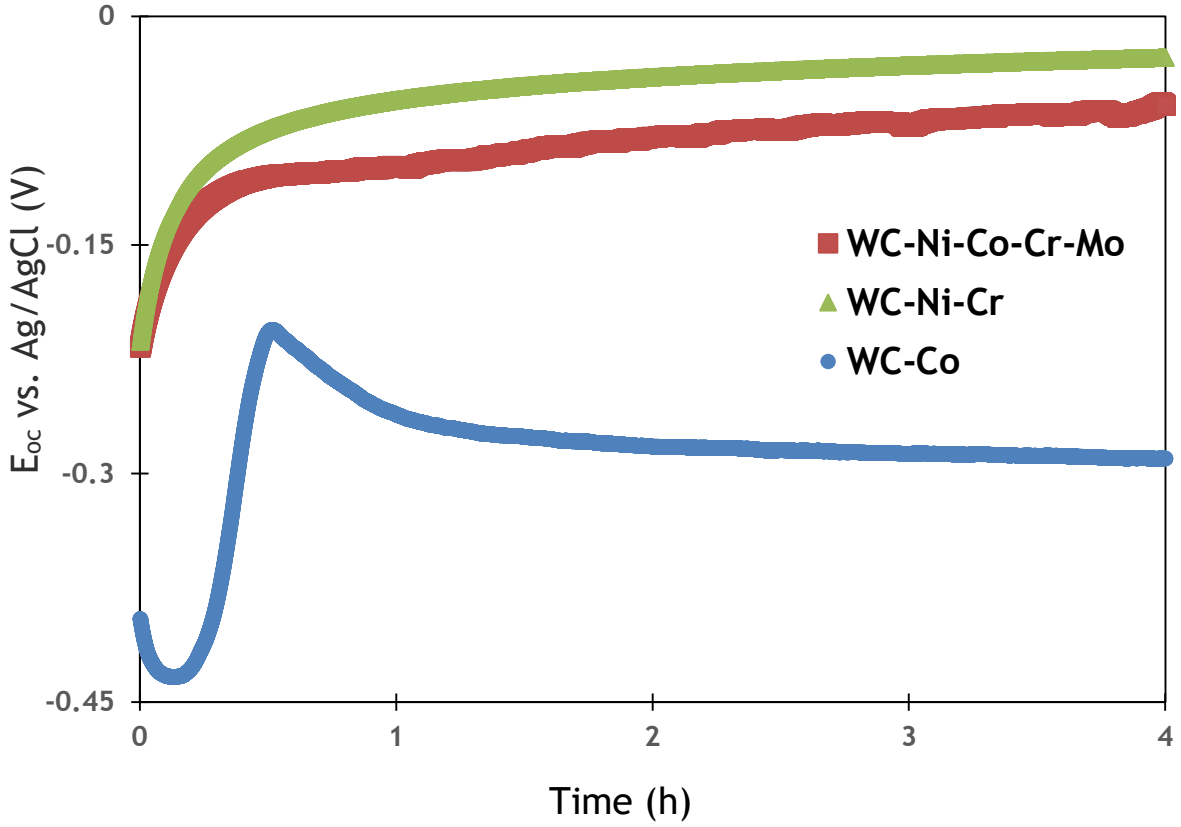

Figure 21 - Open circuit potential measurements for the commercial-grade and intermediate specimens after 4h of immersion.

Table 13 - Open circuit potentials for the commercial-grade and intermediate specimens at the end of 4h of immersion.

	E_{oc} (mV vs. Ag/AgCl)
WC-Ni-Cr	-40
WC-Ni-Co-Cr-Mo	-60
WC-Co	-284

4.3.3. Electrochemical impedance spectroscopy

Corrosion in aqueous environments has a vigorous connection with the characteristics of the interface existent between the material and the media. In most cases, the interface plays the most crucial role in determining if a material is going to have higher or lower corrosion resistance. Material deterioration by metallic dissolution will happen faster as more charge goes through the interface. The greater the corrosion resistance, the less charge the interface allows to go through (by a unit of time). This phenomenon is known as charge transfer resistance or polarization resistance (R_p).

When a protective film is formed on a specimen's surface this usually means there is an interface with elevated R_p.

Impedance (Z) is constituted by the sum of the resistance that the solution offers to ionic migration (R_{sol}) with the impedance of the interface alloy-solution (R_p).

The Bode spectra for the WC-based composites are reported in Fig. 22, Fig. 23, and Fig. 24 and display Bode diagrams obtained after OCP measurements for 4 h of immersion.

The curves that were obtained from the Bode diagrams have simple shapes, and only one constant seems to manifest. With this data, it is possible to use the simple electrical equivalent circuit in Fig. 3 to represent the WC-based composites/solution interface. R_{sol} stands for the solution resistance and R_p stands for film resistance (in cases where there is a passivating film) or for polarization resistance (in cases where there is no protective film) [9].

Surface inhomogeneities or relaxation processes occurring at the interface may take place and roughness of the surface is also a point to be taken, therefore, the capacitive element in parallel with Rp was replaced by a constant phase element (CPE). Y_0 and α are the CPE parameters. A CPE expresses the capability of the interface to store charge in a double layer, similarly to a capacitor [43,44].

The fittings of the EIS data according to the chosen electrical equivalent circuit are plotted in Fig. 22, Fig. 23, and Fig. 24 overlaid on the corresponding experimental data points. The ability of the proposed circuit to describe the experimental data is exceptional (Fig. 22, Fig. 23, and Fig. 24) and the resulting fitting parameters are reported in Table 14 (Z is Impedance and Φ is phase) [9].

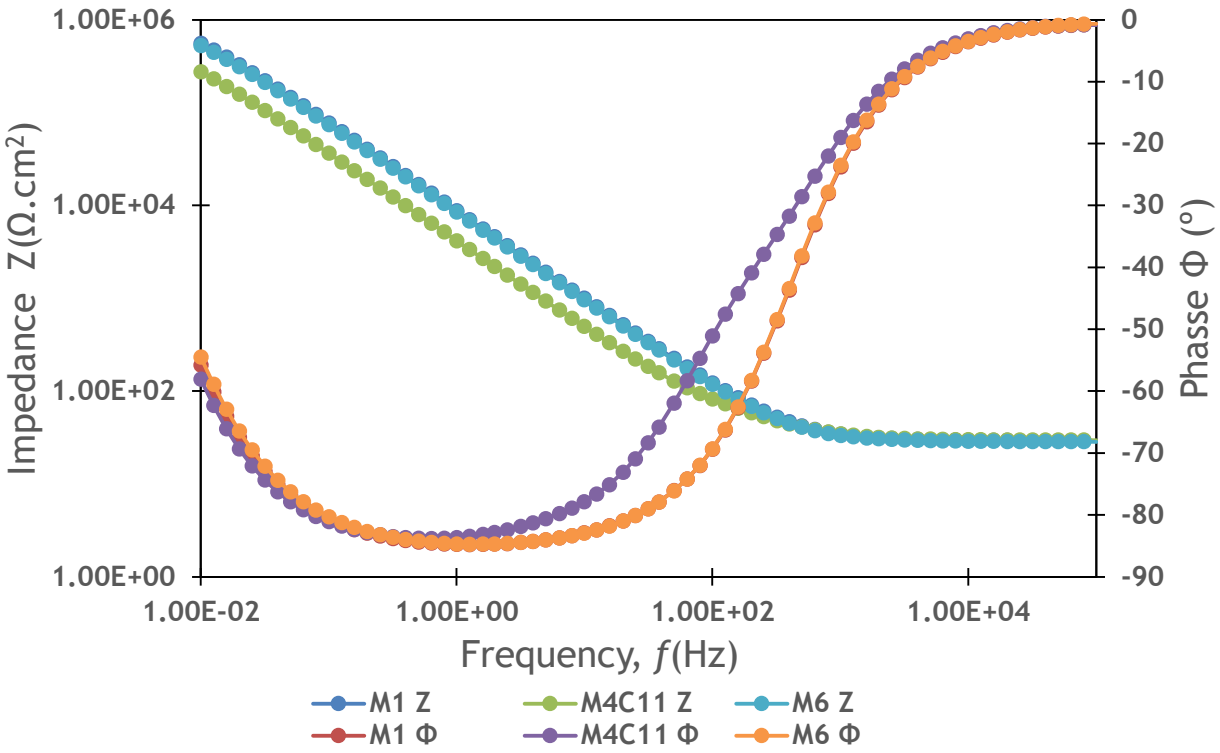

Figure 22 - Bode diagrams of the impedance response obtained for the variation of wt% Mo

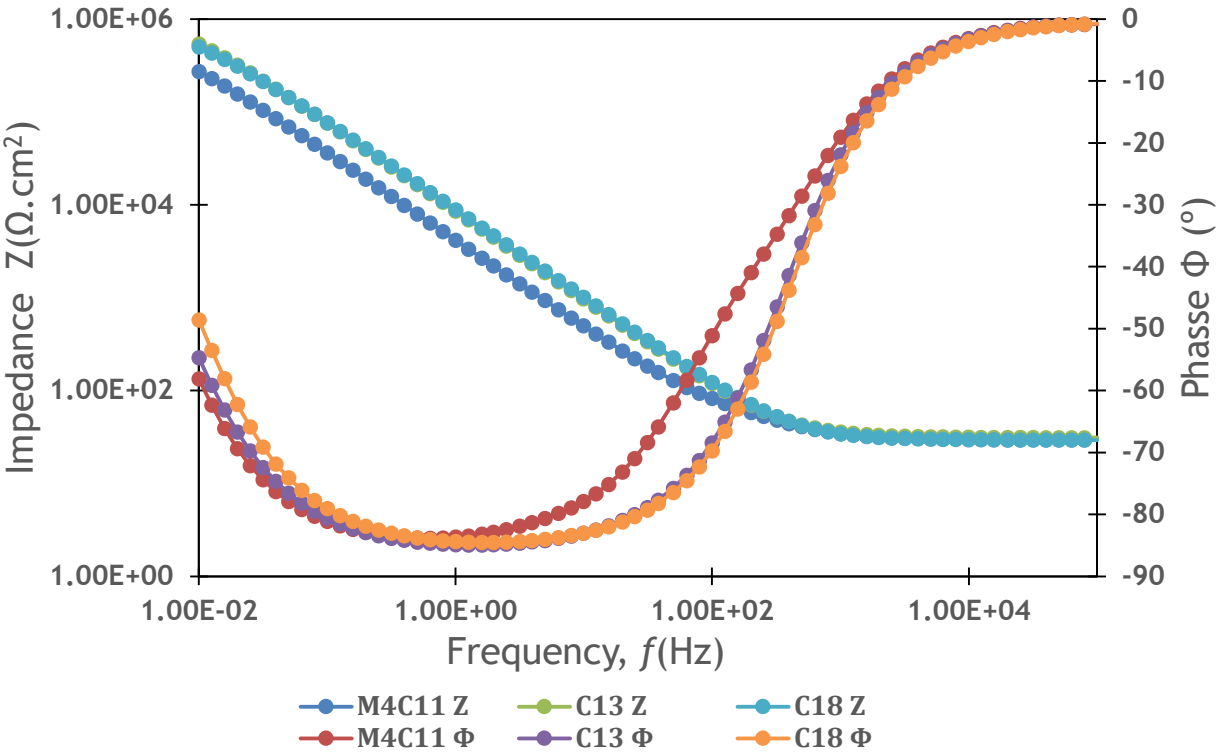

Figure 23 - Bode diagrams of the impedance response obtained for the variation of wt% Cr

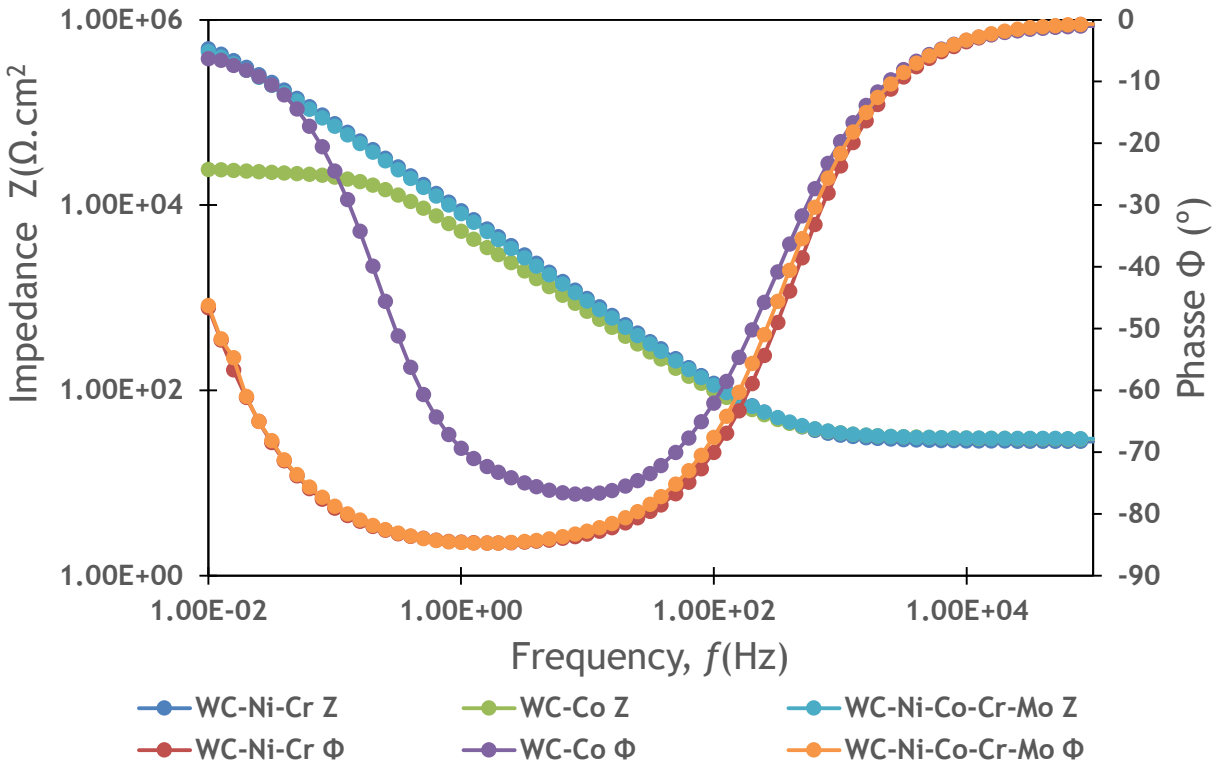

Figure 24 - Bode diagrams of the impedance response obtained for the commercial and the intermediate grades

Table 14 - Solution (R_{sol}) and polarization (R_p) resistances, and CPE parameters (Y0 and α)

	R_{sol} ($\Omega.cm^2$)	R_p ($k\Omega.cm^2$)	α	Y0 ($\mu\Omega^{-1} * s^{\alpha}*cm^{-2}$)
WC-Co	29.7	21	0.90	33.5
WC-Ni-Co-Cr-Mo	29.5	586	0.94	21.4
M4C11	31.0	731	0.93	82.4
C18	29.6	881	0.94	20.5
WC-Ni-Cr	29.7	894	0.94	20.8
C13	31.3	959	0.94	20.5
M6	29.5	1024	0.94	20.9
M1	30.0	1115	0.94	20.4

The α values of the CPE are close to 1, which is associated with an essentially capacitive behaviour of the CPE.

As was expected, the lowest polarization resistance (R_p) value found was for WC-Co followed by the WC-Ni-Co-Cr-Mo specimen. This was also predictable due to the presence of Co in the carbide, which is detrimental to corrosion resistance.

The C18 specimen was expected to score higher since it is the sample with the largest amount of binder. However, it scored right in the middle of the table.

Unexpectedly, M1 and M6 were the two specimens that scored the highest. From the M6 specimen, this was predictable, because, as already demonstrated in the literature, the presence of 0.6 wt% Mo greatly increases corrosion resistance. On the other hand, the highest-scoring specimen was the M1, with it being the lowest wt% of Mo. This is contradictory to what was found in Santos *et al.*, that for chloride media M6 should ranker around three times higher than M1 [9].

These conclusions demonstrate that 0.6 wt% Mo is effective in protecting against corrosion of WC-composites in alkaline chloride media, but intermediate amounts of Mo may contribute to a harmful effect on the corrosion susceptibility of WC-Ni-Cr-Mo alloys. The reasons and the explanation behind such a negative impact could not be provided by this study. Undeniably, a detailed specimen surface analysis after immersion could confirm the presence of any interfacial films, and their structural and chemical characteristics, and could provide insight into such deleterious effects [10].

After 4 h of immersion, the alloys with higher Cr content present a more protective film. M4C11 did not present this fact, and as is explained in the literature, it might develop a discontinuous film that grows in patches and does not render protection. This can happen due to the existence of a more complex interface, possibly a porous film [10].

4.3.4. Potentiodynamic polarization

The voltammograms of the WC-composites are plotted in Fig. 25, Fig. 26 and Fig. 27 and all grades presented a current peak at potentials around -0.3 V.

When analysing Fig. 25 it is clear that the M4C11 specimen had a steeper current peak of about one order of magnitude.

These peaks confirm the low passivation in the presence of chloride and confirms the E_{oc} vs. time behaviour of the specimens.

For the M4C11, C13 and C18 alloys used in this work, Cr represents 10 wt% of the binder which is slightly below the lower limit for corrosion resistance required in stainless steels, yet its effect in promoting a passivated state is still clearly visible here [9,10]. Considering the Mo content variation specimens used for this work, they possess a similar Cr content, which means that the more enhanced active-passive transition of M6 in chloride solution should be attributed to its higher Mo content.

It is noteworthy that, although the increase in Cr content is smaller between C11 and C13, than between C13 and C18, it leads to a far more expressive impact.

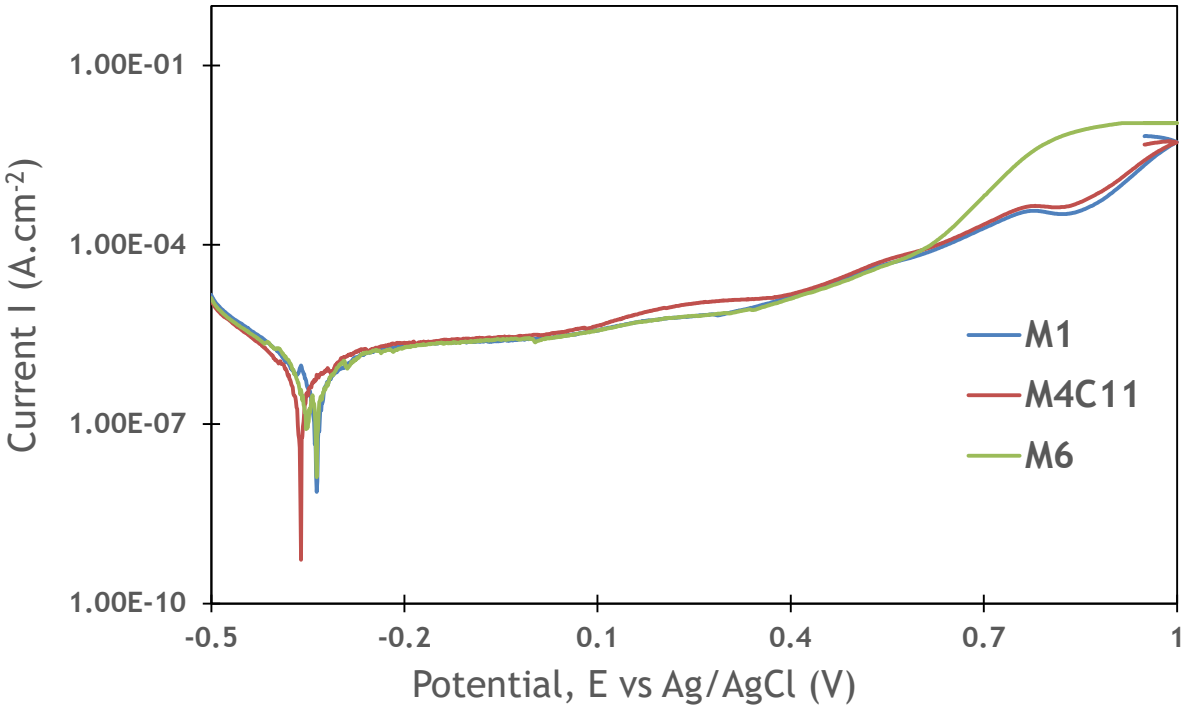

Figure 25 - Potentiodynamic polarization curves obtained for the variation of wt% Mo

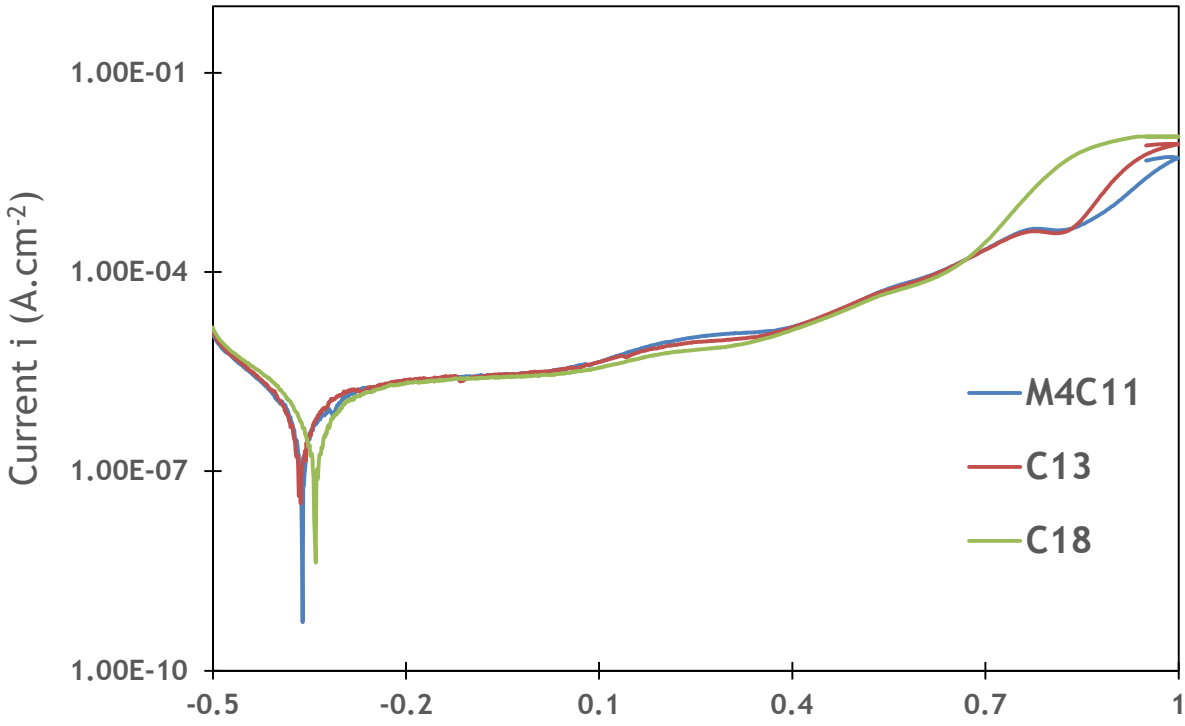

Figure 26 - Potentiodynamic polarization curves obtained for the variation of wt% Cr.

All the specimens have very close values of E_{corr}, however, regarding I_{corr}, the same is not observed. In table 15 it is possible to observe that C13, M6 and WC-Ni-Co-Cr-Mo were the specimens with the lowest I_{corr}, thus, the ones with the best performance regarding corrosion resistance in potentiodynamic polarization.

However, and despite having a higher WC percentage, C18 scored immediately after the first 3 with a very close value for I_{corr}, showing that this specimen is also a very good candidate to applicatiions were corrosion resistance is needed.

As expected WC-Co had very poor results, confirming that this is not a good specimen to be utilized in corrosive media.

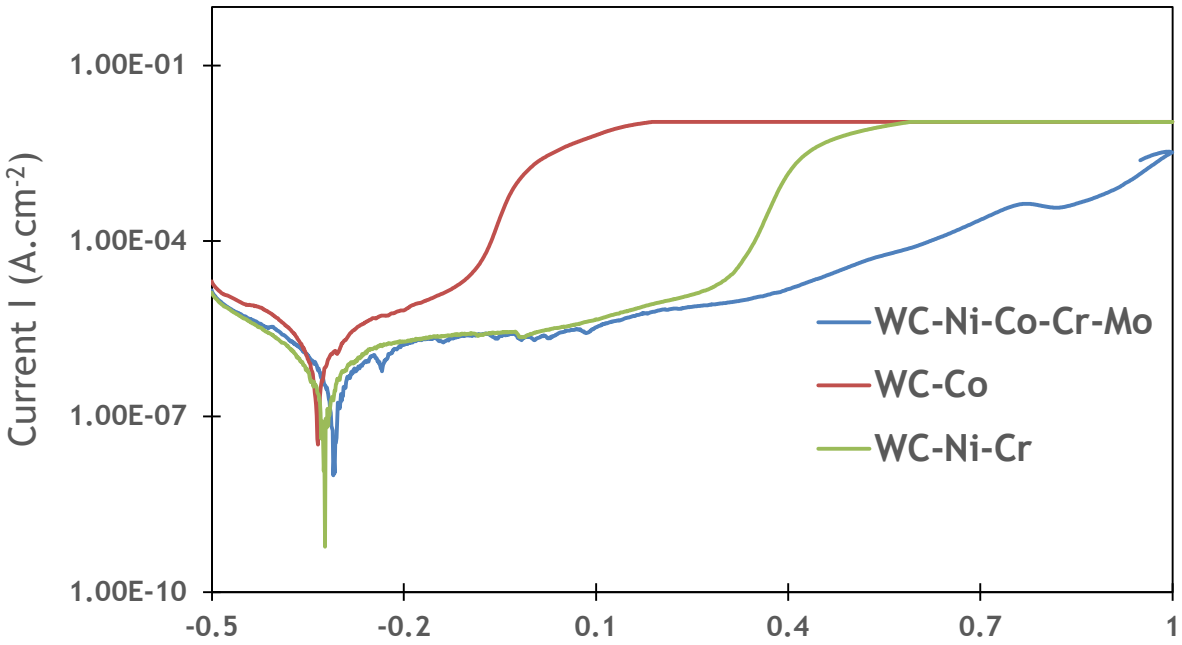

Figure 27 - Potentiodynamic polarization curves obtained for WC-Ni-Co-Cr-Mo, WC-Ni-Cr and WC-Co specimens

Tafel extrapolation was the method used to obtain the values for I_{corr} and it is worth mentioning that this may not be the best method to extract I_{corr} because it assumes activation-controlled reactions which may not always be the cause for the rising in potential. Insulating films on the interface liquid-solid play a big part as well.

As expected, the commercial grade of WC-Co performed very poorly, having the highest values for I_{corr}.

Table 15 – Values of E_{corr} and I_{corr} determined from the Tafel region

	E_{corr} (mV)	I_{corr} (μA)
C13	-351	0.085
M6	-334	0.098
WC-Ni-Co-Cr-Mo	-334	0.100
C18	-304	0.102
WC-Ni-Cr	-309	0.121
M1	-349	0.223
M4C11	-320	0.238
WC-Co	-339	0.241

After completing all 3 experiments all samples had a similar appearance to what is present in Fig. 28.

Figure 28 – specimens' appearance after completion of the 3 experiments

4.4. Composite comparative analysis

In this chapter, a comparative analysis is being made regarding the weighted performance of the studied composites. The volume fraction of the binder has a big impact on the performance of the alloys, so it has to be taken into consideration when comparatively evaluating the specimens. It is not the same to have a specimen with 8.8 wt% binder content with a hardness of 1541 HV30 (C18) and have a specimen with 10 wt% binder content with a hardness of 1577 HV30 (M6). By having a higher wt% of binder with the same or even higher hardness, usually, and without further information, this composite will be preferable. Most probably it will have better corrosion resistance and higher toughness.

In Fig. 29 there is a comparison between Palmqvist toughness in function of hardness, Fig. 29a), and Palmqvist Toughness multiplied by the WC area fraction, in function of Hardness multiplied by the binder's area fraction, Fig 28b).

In Table 16 a comparison is made between the specimens showing a theoretical determination of which one has the best mechanical properties. It was determined through calculation and seriation that the specimens with the best mechanical properties are M4C11, followed by M6, followed by M1. However, and depending on the application, the M6 and M1 specimens may be preferable over the M4C11. This is because they have a lot steadier and constant values.

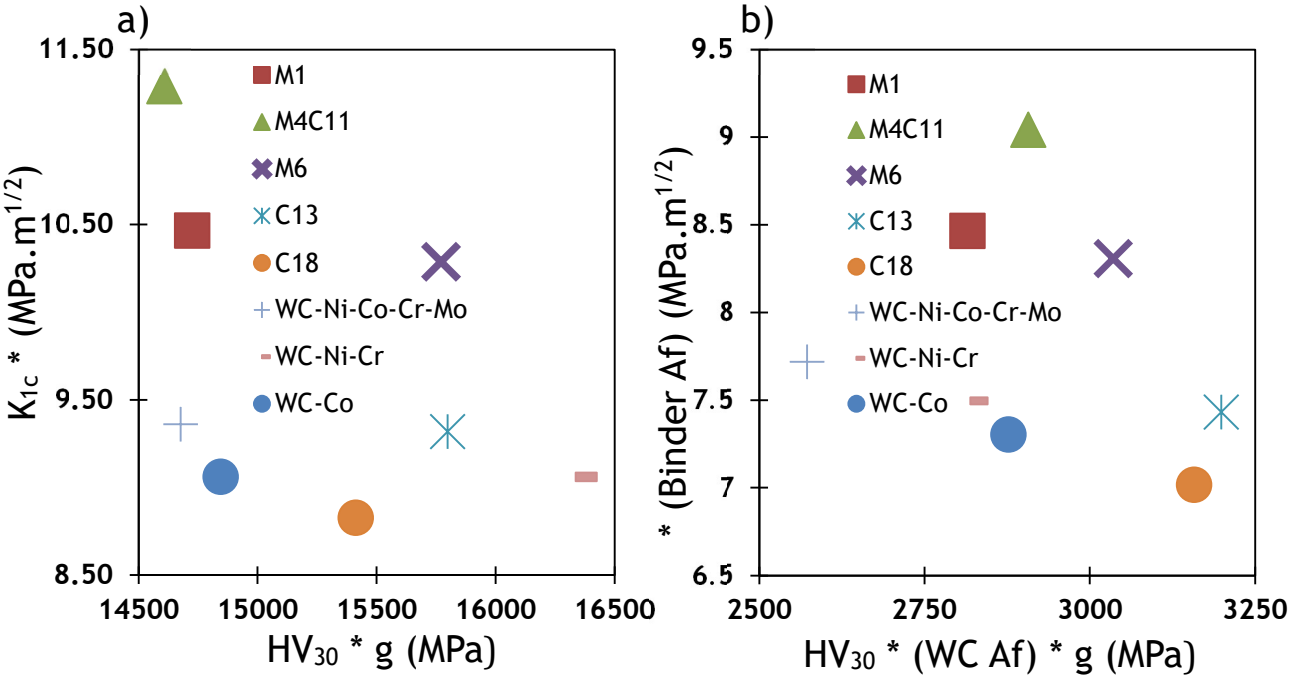

Figure 29 – Graphical representation of the Fracture Toughness in function of Hardness, a), and Fracture Toughness multiplied by the WC area fraction in function of Hardness multiplied by the binder's area fraction, b).

The M4C11, despite having a high K_{1c}, it has a low Hardness performance, which is detrimental for high wear applications. On the other hand, M6 and M1 specimens both have high toughness and high hardness, making them an excellent option for a broader set of applications.

Af stands for area fraction and g stands for gravitational acceleration. This calculation was made to simplify the units used.

Table 16 – Specimens ranking according to the mechanical properties' indicators

Indicators	$K_{1c} * HV_{30} * 10$	$K_{1c} * (1 - Af) * HV_{30} * 10 * Af$	$K_{1c} * (1 - Af)$	$HV_{30} * Af$
Units	$MPa^{2*}\sqrt{m}$	$MPa^{2*}\sqrt{m}$	$MPa*\sqrt{m}$	MPa
M4C11	1.65E+05	2.63E+04	9.0	3.20E+03
M6	1.62E+05	2.52E+04	8.5	3.16E+03
M1	1.54E+05	2.38E+04	8.3	3.04E+03
WC-Ni-Cr	1.48E+05	2.38E+04	7.6	2.91E+03
C13	1.47E+05	2.22E+04	7.5	2.88E+03
WC-Ni-Co-Cr-Mo	1.37E+05	2.14E+04	7.4	2.83E+03
C18	1.36E+05	2.11E+04	7.3	2.82E+03
WC-Co	1.34E+05	2.10E+04	7.0	2.82E+03

In table 17 a comparison is made between the electrochemical properties of the specimens, and they are seriated and ranked according to the values obtained. The values for the modified E_{ocp} took into consideration the lowest scoring specimen, the WC-Co. To obtain these values, firstly the absolute values for the E_{ocp} measurements were calculated. After this, the difference in absolute values between the E_{ocp} value of the WC-Co specimen and the E_{ocp} values of each specimen was added to the base value of the E_{ocp} value of the WC-Co specimen. After this, all obtained values were divided for the E_{ocp} value of the WC-Co specimen. The final result was a pondered E_{ocp} modified value, taking into consideration the lowest value obtained without overly increasing the values in consideration to the WC-Co specimen.

For the case of electrochemical properties, the best specimen was C13 followed by the M6, followed by the C18. These results were mildly expected, due to the high wt% of Cr content, which originates the passivating film on the surface conferring a very high corrosion resistance to the specimens

Despite this observation, the combined values of E_{ocp} and R_p were not the greatest for the C13, this meaning that the M6 and the C18 specimen have a broader range of applications because of their consistency, having both high E_{ocp}, high R_p and low I_{corr} values.

Table 17 – Specimens ranking according to the electrochemical properties' indicators

Indicators	$\frac{E_{ocp} * R_p}{I_{corr}}$	$E_{ocp} * R_p$
Units	$M\Omega * \mu A^{-1}$	$M\Omega$
C13	20.4	2.1
M6	18.8	1.9
C18	16.6	1.8
WC-Ni-Cr	16.4	1.7
M1	9.2	1.7
WC-Ni-Co-Cr-Mo	8.6	1.3
M4C11	5.6	1.1
WC-Co	0.1	0.0

In Table 18 and Fig. 30 a comparison is made between the electrochemical and the mechanical properties of the specimens. To put this into consideration, the higher the values for K_{1c}, HV_{30}, E_{ocp} and R_p the higher the corrosion resistance the specimen has. On the other hand, the lower the I_{corr}, the higher the corrosion resistance as well, and that is why this one is in the denominator. For the neutral chloride media studied, the specimens that behaved the best were M6 and C13, unsurprisingly. Although, and this was not expected, the WC-Ni-Cr specimen ranked third in the list. The C18 specimen also ranked very well with a value of 2.25E+6, meaning it also has good performance regarding corrosion resistance and good mechanical properties

Table 18 – Specimens ranking according to the electrochemical and mechanical properties' indicators

Indicators	$\frac{K_{1c} * HV_{30} * 10 * E_{ocp} * R_p}{I_{corr}}$
Units	$\frac{\mathrm{MPa}^2 * \sqrt{m} * M\Omega}{\mu A}$
M6	3.06E+06
C13	3.01E+06
WC-Ni-Cr	2.43E+06
C18	2.25E+06
M1	1.41E+06
WC-Ni-Co-Cr-Mo	1.19E+06
M4C11	9.24E+05
WC-Co	1.17E+04

The results obtained with these calculations provide realistic and practical feedback regarding the replacement of Co by other binders and makes WC-Ni-Cr-Mo a viable option.

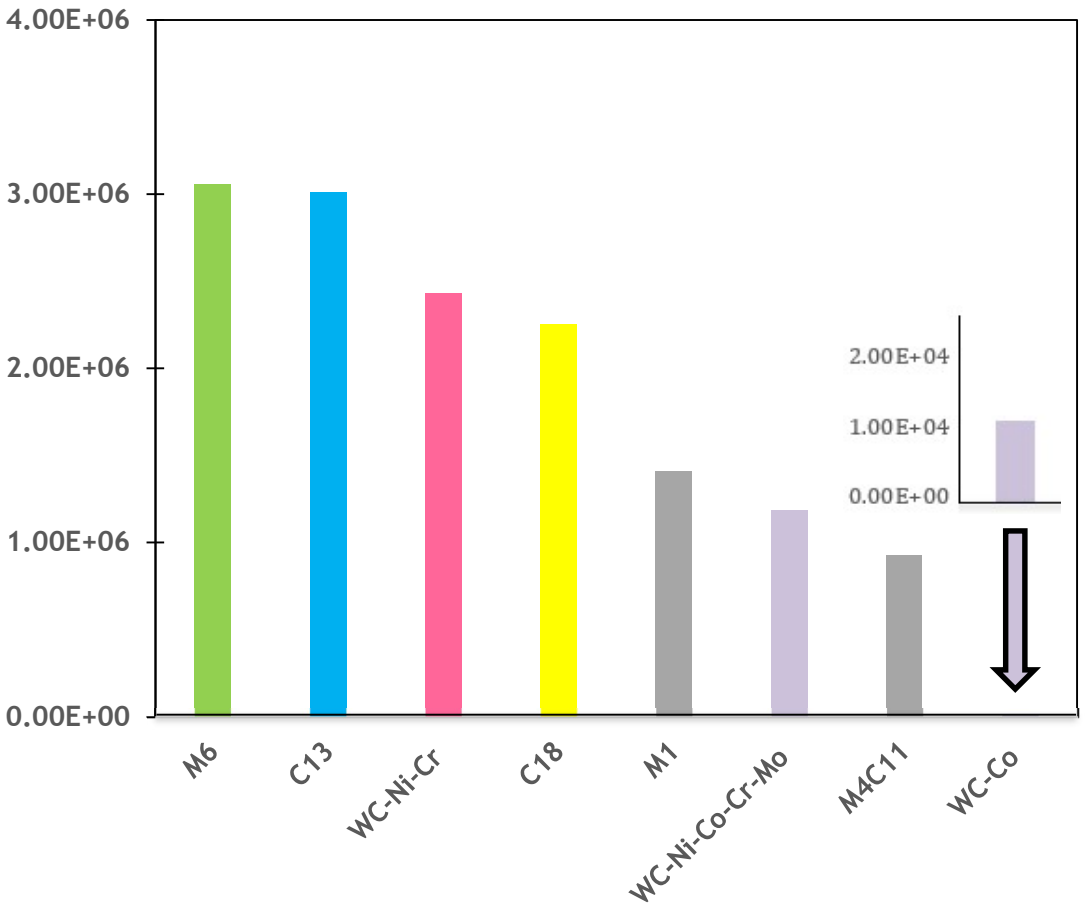

Figure 30 – Graphical representation of the specimens ranking according to the electrochemical and mechanical properties' indicators

5. Conclusions

This work investigated the effect of different Cr and Mo content on the microstructure, mechanical properties, and corrosion resistance of WC-Ni-Cr-Mo composites, in a chloride alkaline media.

The results obtained from open circuit potential measurements, potentiodynamic polarization and EIS, revealed that Cr additions up to 1.8% can effectively decrease corrosion susceptibility in these media without hindering toughness.

As the Cr content increases, the development of a more protective film on the surface of the binder is appointed as the mechanism for higher corrosion resistance.

In the lower Cr content alloy, the development of an insulating barrier from the solution is not as noticeable or a porous film is formed instead, being insufficient to confer high corrosion resistance to the alloy.

Mo presented visible benefits in contents of 0.6 wt% for improved corrosion resistance in WC-Ni-Cr-based composites, effectively enhancing the anodic active-passive transition in chloride medium.

Mo content of 0.6 wt% Mo was also effective in hindering WC grain growth and increasing hardness.

Ni-Cr-Mo is a very interesting candidate to replace Co as a binder for WC-based composites; intermediate additions of 0.4 wt% Mo appear to be detrimental, contributing to a small increase in corrosion susceptibility

The results obtained in this work provide realistic and practical feedback regarding the replacement of Co by other binders. In agreement with the literature [8-10], replacing Co by Ni-Cr-Mo is very much relevant. At some Mo and Cr contents, specifically at 0.6 wt% for Mo content, and over 1.3 wt% of Cr content, it was possible to observe a relevant increase in hardness and an extensive augment in corrosion resistance. These observations come to solve the existing problems regarding the high prices of Co, its high toxicity, and its difficulty to be obtained.

Further, more extensive work should be done on the subject, in order to acquire more data on the specimens. Many applications for cemented carbides, specifically hard metals, involve very corrosive media, it being acidic, alkaline, chlorides, sulphates, etc. Most of them are also applied in environments where increased wear is observed. For that reason, tribocorrosive experiments present one of the main focuses for further investigation and future work.

Referências

[1] S. Norgren, J. García, A. Blomqvist, L. Yin, Trends in the P/M hard metal industry, Int. J. Refract. Met. H., 48 (2015), pp. 31-45, 10.1016/j.ijrmhm.2014.07.007

[2] J. García, V.C. Ciprés, A. Blomqvist, B. Kaplan, Cemented carbide microstructures: a review, Int. J. Refract. Met. H., 80 (2019), pp. 40-68, 10.1016/j.ijrmhm.2018.12.004

[3] X. Ren, H. Miao, Z. Peng, A review of cemented carbides for rock drilling: an old but still tough challenge in geo-engineering, Int. J. Refract. Met. H., 39 (2013), pp. 61-77, 10.1016/j.ijrmhm.2013.01.003

[4] Samuel A. Humphry-Baker, Ke Peng, William E. Lee, Oxidation resistant tungsten carbide hardmetals, Int. J. Refract. Met. H., 66 (2015), pp. 135-143, 10.1016/j.ijrmhm.2017.03.009

[5] L. Leyssens, B. Vinck, C. Van Der Straeten, F. Wuyts, L. Maes, Cobalt toxicity in humans — a review of the potential sources and systemic health effects, Toxicology, 387 (2017), pp. 43-56, 10.1016/j.tox.2017.05.015

[6] P.K. Katiyar, N.S. Randhawa, Corrosion behavior of WC-Co tool bits in simulated (concrete, soil, and mine) solutions with and without chloride additions, Int. J. Refract. Met. H., 85 (2019), p. 105062, 10.1016/j.ijrmhm.2019.105062

[7] Durit – Tecnologia, https://www.durit.com/pt/tecnologia/metal-duro

[8] A.M. Ferro Rocha, A.C. Bastos, J.P. Cardoso, F. Rodrigues, C.M. Fernandes, E. Soares, J. Sacramento, A.M.R. Senos, M.G.S. Ferreira, Corrosion behaviour of WC hardmetals with nickel-based binders, Corros. Sci., 147 (2019), pp. 384-393, 10.1016/j.corsci.2018.11.015

[9] R.F. Santos, A.M. Ferro Rocha, A.C. Bastos, J.P. Cardoso, F. Rodrigues, C.M. Fernandes, J. Sacramento, M.G.S. Ferreira, A.M.R. Senos, C. Fonseca, M.F. Vieira, Luís F. Malheiros, Microstructural characterization and corrosion resistance of WC-Ni-Cr-Mo composite – The effect of Mo, Int. J. Refract. Met. H. 86 (2020) 105090, https://doi.org/10.1016/j.ijrmhm.2020.105434

[10] R.F. Santos, A.M. Ferro Rocha, A.C. Bastos, J.P. Cardoso, F. Rodrigues, C.M. Fernandes, J. Sacramento, M.G.S. Ferreira, A.M.R. Senos, C. Fonseca, M.F. Vieira, Luís F. Malheiros, The effect of Cr content on the corrosion resistance of WC-Ni-Cr-Mo composites, Int. J. Refract. Met. H. 95 (2021) 105434, https://doi.org/10.1016/j.ijrmhm.2019.105090

[11] A.N. Li-cong, C.A.O. Jing, W.U. Lin-cai, M.A.O. Hong-huan, Y.A.N.G. Yi-tao, Effects of Mo and Mn on pitting behavior of duplex stainless steel, J. Iron Steel Res. Int., 23 (2016), pp. 1333-1341, 10.1016/S1006-706X(16)30196-0

[12] A. Pardo, M.C. Merino, A.E. Coy, F. Viejo, R. Arrabal, E. Matykina, Pitting corrosion behaviour of austenitic stainless steels – combining effects of Mn and Mo additions, Corros. Sci., 50 (2008), pp. 1796-1806, 10.1016/j.corsci.2008.04.005

[13] Katsuhisa Sugimoto, Yoshinobu Sawada, The role of alloyed molybdenum in austenitic stainless steels in the inhibition of pitting in neutral halide solutions, Corrosion, 32 (1976), pp. 347-352, 10.5006/0010-9312-32.9.347

[14] R. Qvarfort, Some observations regarding the influence of molybdenum on the pitting corrosion resistance of stainless steels, Corros. Sci., 40 (1998), pp. 215-223, 10.1016/S0010-938X(97)00118-2

[15] R. German, Sintering Theory and Practice, John Wiley & Sons Inc, 1996. https://ui.adsabs.harvard.edu/abs/1996stp..book.....G/abstract

[16] GeneralCarbide®, Sinter-HIP Advantages https://www.generalcarbide.com/wp-content/uploads/2019/04/General-Carbide-Sinter-HIP.pdf

[17] W.J. Tomlinson, N.J. Ayerst, Anodic polarization and corrosion of WC-co hardmetals containing small amounts of Cr3C2 and/or VC, J. Mater. Sci., 24 (1989), pp. 2348-2352, 10.1007/BF01174495

[18] B. Bozzini, G.P. De Gaudenzi, M. Serra, A. Fanigliulo, F. Bogani, Corrosion behaviour of WC-co based hardmetal in neutral chloride and acid sulphate media, Mater. Corros., 53 (2002), pp. 328-334, 10.1002/1521-4176(200205)53:5<328::AID-MACO328>3.0.CO;2-G

[19] K. Shi, K. Zhou, Z. Li, X. Zan, S. Xu, Z. Min, Effect of adding method of Cr on microstructure and properties of WC–9Ni–2Cr cemented carbides, Int. J. Refract. Met. H., 38 (2013), pp. 1-6, 10.1016/j.ijrmhm.2012.11.010

[20] G. Li, Y. Peng, L. Yan, T. Xu, J. Long, F. Luo, Effects of Cr concentration on the microstructure and properties of WC-Ni cemented carbides, J. Mater. Res. Technol., 9-1 (2020), pp. 902-907, 10.1016/j.jmrt.2019.11.030

[21] R.O. Calderon, C. Edtmaier, W. Schubert, Novel binders for WC-based cemented carbides with high Cr contents, Int. J. Refract. Met. H., 85 (2019), p. 105063, 10.1016/j.ijrmhm.2019.105063

[22] P.K. Katiyar, A comprehensive review on synergy effect between corrosion and wear of cemented tungsten carbide tool bits: a mechanistic approach. Int. J. Refract. Met. H., 92 (2020), p. 105315, 10.1016/j.ijrmhm.2020.105315

[23] C.G. Garay-Reyes, M.A. Ruiz-Esparza-Rodríguez, J.M. Mendoza-Duarte, I.E. Guel, S.E. Hernández-Martínez, J.L. Hernández-Rivera, J.J. Cruz-Rivera, J.S. Castro-Carmona, H.M. Medrano-Prieto, J.M. Silva-Aceves, H. Camacho-Montes, Q. Estrada, R. Martínez-Sánchez, Effect of Fe impurities and pure Cr additions on microstructure of nanostructured WC-10Co alloy sintered by HIP, J. Alloys Compd., 800 (2019), pp. 462-467, 10.1016/j.jallcom.2019.06.045

[24] Lukas Lauter, Roman Hochenauer, Chirstoph Buchegger, Marcel Bohn, Walter Lengauer, Solid-state solubilities of grain-growth inhibitors in WC-Co and WC-MC-Co hardmetals, J. Alloy Compd., 675 (2016), pp. 407-415, 10.1016/j.jallcom.2016.03.117

[25] S.G. Huang, J. Vleugels, H. Mohrbacher, M. Woydt, Microstructure and tribological performance of NbC-Ni cermets modified by VC and Mo2C, Int. J. Refract. Met. H., 66 (2017), pp. 188-197, 10.1016/j.ijrmhm.2017.03.012

[26] S. Guo, J. Yang, H. Chen, J. Yi, Effect of Mo and Y2O3 additions on the microstructure and properties of fine WC-co cemented carbides fabricated by spark plasma sintering, Int. J. Refract. Met. H., 69 (2017), pp. 1-10, 10.1016/j.ijrmhm.2017.07.010

[27] R.M. Genga, L.A. Cornish, G. Akdogan, Effect of Mo2C additions on the properties of SPS manufactured WC-TiC-Ni cemented carbides, Int. J. Refract. Met. H., 41 (2013), pp. 12-21, 10.1016/j.ijrmhm.2013.01.008

[28] C.R. Clayton, Y.C. Lu, A bipolar model of the passivity of stainless steel: the role of Mo addition, J. Electrochem. Soc., 133 (1986), pp. 2465-2473, 10.1002/chin.198714026

[29] Y.C. Lu, C.R. Clayton, A.R. Brooks, A bipolar model of the passivity of stainless steels—II. The influence of aqueous molybdate, Corros. Sci., 29 (1989), pp. 863-880, 10.1016/0010-938X(89)90058-9

[30] M. Kaneko, H.S. Isaacs, Effects of molybdenum on the pitting of ferritic- and austenitic-stainless steels in bromide and chloride solutions, Corros. Sci., 44 (2002), pp. 1825-1834, 10.1016/S0010-938X(02)00003-3

[31] N. Boucherit, A. Hugot-Le Goff, S. Joiret, Influence of Ni, Mo, and Cr on pitting corrosion of steels studied by Raman spectroscopy, Corrosion, 48 (1992), pp. 569-579, 10.5006/1.3315974

[32] A. Tomio, M. Sagara, T. Doi, H. Amaya, N. Otsuka, T. Kudo, Role of alloyed molybdenum on corrosion resistance of austenitic Ni-Cr-Mo-Fe alloys in H2S-Cl− environments, Corros. Sci., 98 (2015), pp. 391-398, 10.1016/j.corsci.2015.05.053

[33] N. Lin, C.H. Wu, Y.H. He, D.F. Zhang, Effect of Mo and Co additions on the microstructure and properties of WC-TiC-Ni cemented carbides, Int. J. Refract. Met. H., 30 (2012), pp. 107-113, 10.1016/j.ijrmhm.2011.07.011

[34] Qiankun Zhang, Nan Lin, Yuehui He, Effects of Mo additions on the corrosion behavior of WC-TiC-Ni hardmetals in acidic solutions, Int. J. Refract. Met. H., 38 (2013), pp. 15-25, 10.1016/j.ijrmhm.2012.12.003

[35] A. Pardo, M.C. Merino, A.E. Coy, F. Viejo, R. Arrabal, E. Matykina, Effect of Mo and Mn additions on the corrosion behaviour of AISI 304 and 316 stainless steels in H_2SO_4, Corros. Sci., 50 (2008), pp. 780-794, 10.1016/j.corsci.2007.11.004

[36] Jun Shu, Hongyun Bi, Xin Li, Zhou Xu, The effect of copper and molybdenum on pitting corrosion and stress corrosion cracking behavior of ultra-pure ferritic stainless steels, Corros. Sci., 57 (2012), pp. 89-98, 10.1016/j.corsci.2011.12.030

[37] S.J. Doh, J.H. Je, J.S. Kim, K.Y. Kim, H.S. Kim, Y.D. Lee, J.M. Lee, Y. Hwu, Influence of Cr and Mo on the passivation of stainless steel 430 (18Cr) and 444 (18Cr-2Mo): in situ XANES study, Nucl. Instrum. Method B., 199 (2003), pp. 211-215, 10.1016/S0168-583X(02)01548-3

[38] A. Boukantar, B. Djerdjare, F. Guiberteau, A L. Ortiz, A critical comparison of the tribocorrosive performance in highly-alkaline wet medium of ultrafine-grained WC cemented carbides with Co, Co+Ni, or Co+Ni+Cr binders, Int. J. Refract. Met. H. 95 (2021) 105452, https://doi.org/10.1016/j.ijrmhm.2020.105452

[39] S. Mischler, A.I. Munoz, Tribocorrosion, Encyclopedia of Interfacial Chemistry (2018) 504-514
https://www.sciencedirect.com/science/article/pii/B9780124095472134249

[40] Gamry Instruments, 2022, "Open Circuit Potential", accessed 25th of March 2022, https://www.gamry.com/Framework%20Help/HTML5%20-%20Tripane%20-%20Audience%20A/Content/UT/Open%20Circuit%20Potential.htm

[41] Gamry Instruments, 2022, "Basics of Electrochemical Impedance Spectroscopy", accessed 25th of March 2022, https://www.gamry.com/application-notes/EIS/basics-of-electrochemical-impedance-spectroscopy/

[42] Gamry Instruments, 2022, “Integrating Cyclic Voltammetry: How and Why”, accessed 25th of March 2022, https://www.gamry.com/application-notes/physechem/cyclic-voltammetry-integrating-cv/

[43] P. Córdoba-Torres, Relationship between constant-phase element (CPE) parameters and physical properties of films with a distributed resistivity, Electrochim. Acta, 225 (2017) 592–604, https://doi.org/10.1016/j.electacta.2016.12.087.

[44] C.M. Fernandes, A. Rocha, J.P. Cardoso, A.C. Bastos, E. Soares, J. Sacramento, M.G.S. Ferreira, A.M.R. Senos, WC-stainless steel hardmetals, Int. J. Refract. Met. H. 72, (2018) 21–26, https://doi.org/10.1016/j.ijrmhm.2017.11.046